Available online at www.sciencedirect.com
ScienceDirect
Trans. Nonferrous Met. Soc. China 33(2023) 865−888
Transactions of Nonferrous Metals Society of China
www.tnmsc.cn

Present-day state of tectonic stress and tectonization in coastal gold mine area near Laizhou Gulf, North China

Peng LI[1,2,3], Qi-feng GUO[1,2,3], Mei-feng CAI[1,2,3], Sheng-jun MIAO[1,2,3]

1. School of Civil and Resources Engineering, University of Science and Technology Beijing, Beijing 100083, China;
2. Key Laboratory of High-Efficient Mining and Safety of Metal Mines, Ministry of Education, University of Science and Technology Beijing, Beijing 100083, China;
3. Beijing Key Laboratory of Urban Underground Space Engineering, University of Science and Technology Beijing, Beijing 100083, China

Received 2 December 2021; accepted 8 June 2022

Abstract: To investigate the present-day state of tectonic stress and tectonization in a coastal gold mine area near the Laizhou Gulf, North China, overcoring, anelastic strain recovery, and hydraulic fracturing stress measurement campaigns were performed, and a total of 49 groups of stress data were determined. The results indicate that horizontal tectonic stress plays a predominant role in the present-day stress field, which is a typical tectonic stress field. The stress fields are characterized by $\sigma_H>\sigma_h>\sigma_v$ (σ_H, σ_h and σ_v are the maximum horizontal, minimum horizontal and vertical principal stresses, respectively) and $\sigma_H>\sigma_v>\sigma_h$, which appear to favor thrust and strike-slip faulting, respectively. The stress level is relatively high and is not conducive to the stability of underground excavations. σ_H is oriented in the WNW−ESE or approximately E−W directions, which is in accord with that indicated by focal mechanism solutions and regional geological structure analysis. The contemporary stress field is the result of dynamic action and tectonic movement in various geological periods; the contemporary stress field generally inherited the characteristics of the third stage tectonic stress field (Himalayan movement period) while partially retaining the characteristics of the second stage tectonic stress field (Yanshanian period), and finally evolved into the tectonic stress field characterized by nearly E−W extrusion.
Key words: in situ stress measurement; present-day stress field; tectonization; fault structure; coastal gold mine area

1 Introduction

The contemporary stress field is formed under the joint action of historical multistage tectonism and neotectonic activity, which directly affects and even controls crustal movement and geological processes [1−4]. Due to the complexity of the continental tectonic framework and heterogeneity of the crustal solid medium, the distribution of the crustal stress field is inhomogeneous. The deformation and failure of the Earth's surface, tectonic movement in the crust, and various geological disasters are closely associated with the crustal stress field [5−7]. In addition, crustal stress is also the critical driving force triggering instability in underground rock engineering [8−10], such as mines and hydropower stations. Therefore, full knowledge of the stress state and its variation pattern in the region of interest is crucial to the study of rock engineering stability, tectonic activities, and geological disasters, such as earthquakes, in the region [11]. Because the constitutive relation of the rock medium in different geological periods is unclear, a complete theoretical description is almost impossible. Thus, research work related to the modern tectonic stress field must depend on the in situ stress measurement results.

Corresponding author: Peng LI, Tel: +86-10-62333700, E-mail: pengli@ustb.edu.cn
DOI: 10.1016/S1003-6326(23)66152-7

The applications of in situ stress measurements have been carried out in many aspects of engineering and geoscience research. ZOBACK [12] investigated the relationship between the stress field and the structure of individual regions and established first-order and second-order models of crustal stress. ZANG et al [13] discussed the relationship between vertical stress components and horizontal stress coefficients of different rock types and depths and studied the stress ratio related to the depth, lithology, and faulting state. MIAO et al [14] analyzed the distribution pattern of the in situ stress field and the evolution characteristics of the geological structure in a gold mining area and gained insight into their relationship. RAJABI et al [15] described the current tectonic stress state in the Darling Basin, Australia, and discussed the significance of stress measurements in resource exploration and production. HAN et al [16] determined the characteristics of the in situ stress field in the Kaiping coalfield and explored the mechanism of large syncline influences on the stress field. MIAO et al [17] proposed a prediction method for rock bursts in metal mines based on in situ stress measurements and energy accumulation theory. LI et al [18] analyzed the distribution characteristics of the stress field around the Yishu fault zone in China and preliminarily evaluated its activity. The above research provides valuable experience for exploring solid earth science, the stability of underground engineering, and the safe and efficient development of mineral resources from the perspective of in situ stress and further highlights the significance of in situ stress measurements.

A coastal gold mine is geographically located adjacent to the Laizhou Gulf in Jiaodong Peninsula, Shandong Province, North China, surrounded by the Bohai Sea on three sides and connected only to the hinterland in the southeast. The mined ore bodies all exist beneath sea level, and the current average mining depth is deeper than 1000 m. Moreover, the gold mine area is located at the intersection of the North China plate, Yangtze plate, and Pacific plate, where the Pacific tectonic domain is combined with the Sulu ultrahigh pressure metamorphic belt and is bounded by a large strike-slip fault zone (i.e., Tan–Lu fault zone), and the gold mine area is adjacent to the western Shandong region (Fig. 1) [19]. Consequently, the geological structural environment in the mine area is quite complex, and seismicity in the surrounding areas, especially in the Laizhou Gulf, is fairly frequent. Moreover, due to the complex tectonic background and engineering disturbance, the frequency of engineering dynamic disasters such as rock bursts is high, and roadway support is extremely difficult, all of which pose a major threat to the safe mining of deep resources.

Under these circumstances, ensuring safe and efficient mining is a difficult problem. To reliably assess the mining dynamics and stability of the mining system and thus ensure the safety of mining operations, multistage stress measurement campaigns have been performed recently in the mine area by using an improved overcoring stress

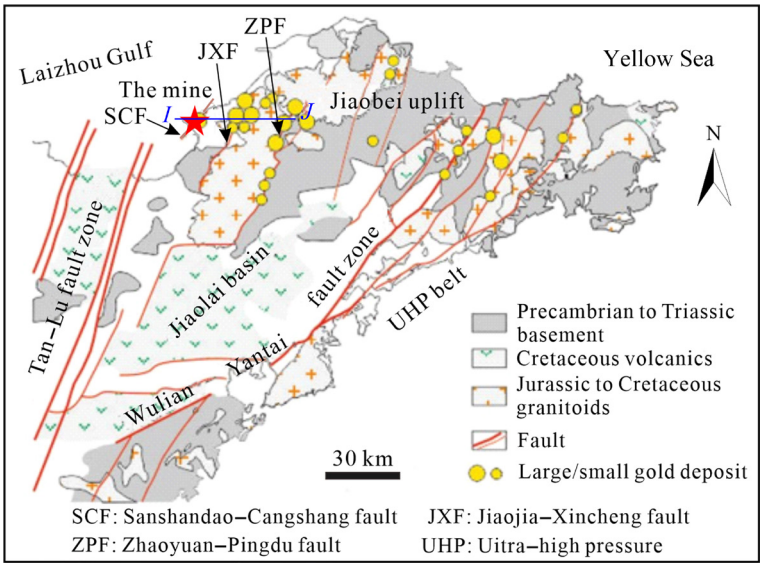

Fig. 1 Map showing general geology around gold mine (after LIU et al [19])

measurement technique, anelastic strain recovery method, and hydraulic fracturing method. As a result, a large body of valuable and reliable stress data was determined. Accordingly, in the present study, the distribution features of the present-day stress field in the mine area were determined using the new compilation of three types of in situ stress measurements, and the relation between the stress field and tectonization was systematically investigated through geological structure analysis, which provides a marvelous opportunity to gain insight into the engineering stability, tectonic movement evolution, and geodynamic processes in the mine area.

2 Geological setting

Tectonically, the gold mine area is located near the southeast edge of the North China Craton. During its long geological history, the mine area has experienced multiple tectonic movements, and the structural development and evolution have mainly experienced three stages, namely, the Mesozoic Indosinian movement and Yanshan movement and the Cenozoic Himalayan movement [20]. The multistage tectonic evolution has formed a complex and changeable structural unit pattern and various diagenetic and metallogenic environments in the mine area. Moreover, the multicycle tectonic movement has resulted in the superposition of magmatism, metamorphism, and mineralization in this area [21]. In the Mesozoic, this area experienced complex tectonic stress transformation, which directly affected the large-scale gold mineralization in the area. Moreover, many small and large gold deposits are also distributed near the area (Fig. 1). The terrain of the mine area is low and flat, with average altitudes of 2−3 m. The rock formation in the area is simple, and the stratigraphic lithologies are plagioclase amphibolite, biotite granulite, gneiss, and trondhjemite−tonalite−granodiorite (TTG) rock series of the Guogezhuang Formation of the Neoarchean Jiaodong Group, and most of them are covered by seawater and Quaternary sediments [22]. This region is characterized by Precambrian basement and Mesozoic magmatic rocks. The exposed intermediate-basic dikes in the area are mainly diabase, diabase porphyrite and lamprophyre, and the magmatic rocks are primarily Yanshanian granites, including Linglong monzogranite and Guojialing granodiorite (Fig. 2(a)) [23]. The ore bodies are generally distributed in pyrite sericite altered rocks in the footwall of the Sanshandao–Cangshang fault zone, and the main ore lithologies are pyrite sericite cataclastic rock, pyrite sericite granitic cataclastic rock, and sericite granite.

The geological structures in the area are dominated by faults, and the NE- and NW-trending faults are two of the group faults that have been well developed (Fig. 2(b)). The NE-trending faults are mainly premineralization faults with multistage activity and are the main ore-controlling faults, as represented by the Sanshandao–Cangshang fault (F1) [24,25]. F1 generally strikes 35°, inclines to the SE, and dips 35°−50°, showing an “S” shape horizontally. The main section presents a gentle wave shape, with 2−10 m thick structural cataclastic rock belts developed on both sides and altered rock belts developed outward (Fig. 2(c)). Blocked by fault gouges in the fault plane, the altered rock belt in the footwall (approximately

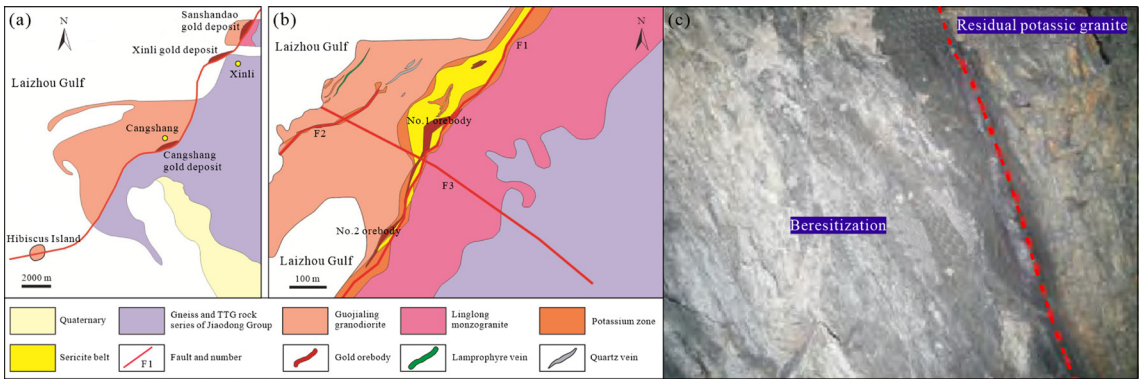

Fig. 2 Geologic maps of Sanshandao–Cangshang fault (a) and mine area (b) and structurally oriented beresite along main section of F1 fault (the hanging wall is weakly mineralized and altered, and the residual potassic granite remains) (c) (after QIU et al [22])

200 m wide) is much wider than that in the hanging wall (only 20 m in width) [22]. This fault controls almost all the proven large and superlarge gold deposits in the area, and only a few small gold deposits are distributed to the east of the fault. The wall rocks on both sides of the fault have strong alteration and obvious zoning, which are the pyritized sericitized zone, potassium zone, and unaltered granite from inside to outside [26]. The secondary fault F2 of F1 basically coincides with the strike of F1 and tends to be the same or opposite to F1. The NW-trending faults are represented by the Sanshandao–Sanyuan fault (F3). F3 is the most important NW-trending fault structure, most of which is developed in this mine area. It extends beyond the mine area in the SE direction and to the Laizhou Gulf in the NW direction, with a total exposed length of approximately 1500 m in the mine area. The overall strike of F3 is 290°−300°, the inclination is NE, and the dip angle is steep (greater than 80°) in some sections. The fault crosses the mine area and extends more than 600 m underground. The above three faults constitute the basic structural framework of the area.

3 Seismicity and regional tectonic stress field

Since the Mesozoic, the Laizhou region has experienced severe tectonic movements (i.e., Indosinian, Yanshan, and Himalayan movements). As a consequence, the seismicity in the Laizhou region and its offshore area is remarkable and prominent. The special geographical location and complex geological structural background determine that these areas are seismically active zones. The intersection of faults in different directions constitutes the seismogenic structure of moderate and small earthquakes in those areas. The Laizhou region and adjacent areas inherit the basic characteristics of historical seismicity, are the areas with high incidences of moderate and small earthquakes and earthquake swarms, and are also some of the intersection areas with the most frequent seismicity in North China [27]. Since earthquakes were recorded, micro, small, and moderate earthquakes have occurred many times in inland Laizhou and surrounding areas [28−30], such as the Ms 4.1 earthquake in 1993, Ms 3.8 earthquake in 2012, Ms 4.6 earthquake in 2013, Ms 4.9 earthquake in 2013, and Ms 2.2 earthquake in 2015 in inland Laizhou, as well as the Ms $4^{3}/_{4}$ earthquake in 1346, Ms $6^{1}/_{2}$ earthquake in 1945, and Ms 3.9 earthquake in 1983 in the Laizhou Gulf. From 1970 to 2013, more than 1000 earthquake events of Ms ≥ 2.0 occurred in the study area and its adjacent areas (Fig. 3(a)). The focal depth ranges from 3 to 48 km. The seismic activity is unevenly distributed in space and is obviously controlled by regional active faults, especially those with large scales, such as the Tan–Lu fault zone, and is also greatly influenced by the strong earthquake activity in Japan located in the subduction zone of the Pacific plate. The frequent occurrence of moderate and small earthquakes around the mine area indicates that this area is an active area of modern

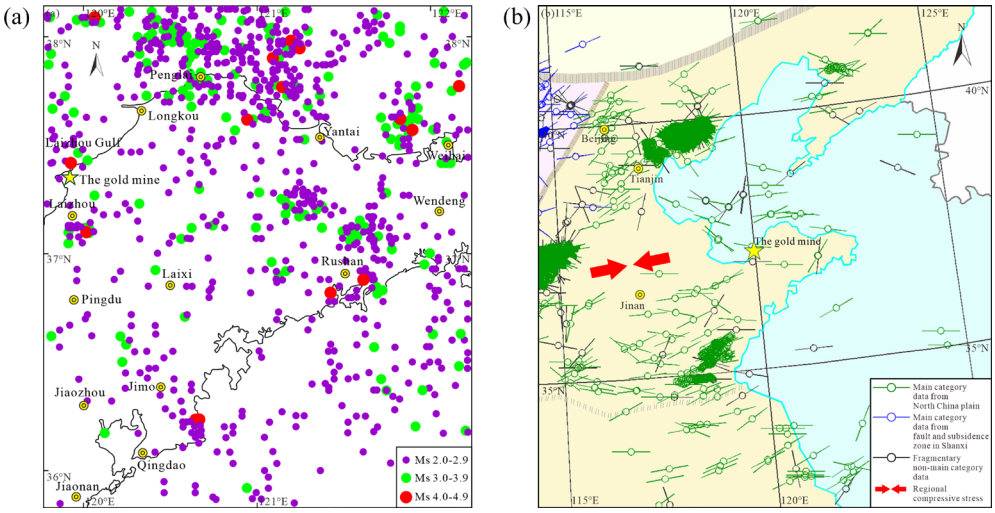

Fig. 3 Distribution of earthquakes of Ms ≥ 2.0 around mine area since 1970 (a) and tectonic stress map in North China derived from focal mechanism solutions (b) (after KANG et al [31])

tectonization.

Based on the plate motions and the interpretations of deep focal mechanism solutions of earthquakes, the distributions of the regional principal compressive stresses in North China are characterized and depicted in Fig. 3(b) [31]. The regional compressive stress directions around the mine area, which are indicated by focal mechanism solutions, are dominantly oriented in the WNW–ESE or nearly E−W orientations, even though the existing data are small. In addition, a large number of focal mechanism data [32,33] compiled around the mine area indicate that, in recent decades, the orientation of the tectonic stress field in the Laizhou region and adjacent districts has been relatively stable with the principal compressive stress directions of WNW−ENE or approximately E−W, and the tectonic movement is mainly horizontal. Similarly, a recent focal mechanism investigation of the Ms 4.6 in 2013 earthquake that occurred in the Laizhou region [30] demonstrates a WNW−ESE azimuth for the nearly horizontal principal compressive stress.

4 Methodology used to determine stress tensors in mine area

4.1 Improved overcoring technique for stress measurements

The overcoring method, recommended by the Test Methods Committee of the International Society for Rock Mechanics (ISRM) [18], is a relatively mature technique that has been developed over decades. It is the only method that can accurately determine the 3D original rock stress state at a point in a single borehole and has excellent applicability and reliability when measuring the original stress. According to statistics, approximately 80% of the in situ stress data all over the world are measured by this method. In general, the overcoring method can determine complete stress tensors from the borehole diametric change during overcoring and subsequent stress relaxation based on elasticity theory. With knowledge of the recovery strain and the in situ mechanical parameters of the core, the value and azimuth of the stress acting on the rock mass can be calculated. For mines, the overcoring method is more advantageous because there are a series of tunnels and chambers in the mine that can approach the underground measuring points, and there is no need to drill special holes to reach the measuring points, which is the case with the hydraulic fracturing method. Therefore, the overcoring method is an economical and reliable technique for in situ stress measurement in mines.

4.1.1 Improvements to overcoring technique

In deep mining, the conventional overcoring method based on linear elastic theory cannot adapt to the development of deep rock mechanics research and meet the requirements of deep measurements because the deep rock mass has more remarkable mechanical characteristics of nonlinearity, heterogeneity, and anisotropy compared with the shallow rock mass. Furthermore, the deep rock mass is of poorer quality and in a higher geothermal environment. On the other hand, the resistance strain gauge is very sensitive to temperature. When the temperature changes, the resistance value changes accordingly, and the corresponding output voltage is generated in the bridge, resulting in the calculated false additional strain value. Consequently, temperature is an influential factor that cannot be ignored for in situ stress measurements. However, it is difficult for ordinary hollow inclusion strain gauges to eliminate the influence of temperature changes on the measurement results, which leads to notable errors in the measurement results. Additionally, the conventional temperature compensation method cannot reduce the error caused by large temperature changes in deep strata and meet the requirements of accurate measurement in complex geological environments. To eliminate the additional strain caused by temperature changes, appropriate methods must be adopted to compensate or correct for the influence of temperature, which is of great significance to ensure the accuracy of in situ stress measurement results. For those purposes, some improvements to the traditional overcoring technique have been made and are introduced as follows [17,34−36].

(1) Based on the original installation equipment, a camera device built into the borehole was configured; this device can observe the damage of the rock mass at different depths in the borehole, master the quality of the rock mass at the installation position of the strain gauge, and effectively avoid the unsatisfactory installation or even the failure of strain gauge installation caused

by rock mass breakage.

(2) A new complete temperature compensation technique was invented by CAI et al [35], and the design and structure of the hollow inclusion strain gauge were improved accordingly (Fig. 4(a)) [9]. The specific improvements of the hollow inclusion strain gauge are as follows: (a) a thermistor is embedded at point *D* between strain rosettes *A* and *C* to measure the temperature change at the measuring point during overcoring; (b) To eliminate the additional strain caused by the resistance strain gauge wire temperature change, two no-load wires, which are the same as the resistance strain gauge wire, are welded together at point *E* and are led out from the cable together with other strain gauge wires and connected into the bridge arm adjacent to the working strain gauge. In this way, when the temperature changes, the resistance changes in two adjacent bridge arms are the same due to the same length of wires so that they can offset each other. In addition, the temperature calibration test in a thermostat with adjustable temperature is added after each stress relief test is completed, and practice has shown that effective complete temperature compensation can be realized.

(3) Automatic strain measurement and recording system. A new strain−resistance−voltage conversion device was developed and used in the measurements, and a new data collector was also adopted in the recording device for continuous and automatic recording, which can simultaneously record the data of 48 channels within 1×10^{-4} s, thus ensuring the accuracy of recording.

(4) The calculation of in situ stresses for the overcoring method needs to be solved by the double iteration method. Consequently, a 3D in situ stress inversion program involving the double iterative algorithm was independently developed to solve the rock elastic modulus, Poisson ratio, *K* value (*K* is the correction coefficient), and the in situ stress value, thereby ensuring the reliability and accuracy of the calculation processes and results.

Overall, the improved overcoring technique can realize complete temperature compensation and consider the nature of actual rock masses, and the technique was employed to measure the stress in the gold mine. Because a series of new technologies, setups, and approaches were used in the measurement process to improve the measurement accuracy, the reliability of the measurement results has been greatly improved.

4.1.2 Stress measurement process and results

The accuracy of in situ stress measurement results is not only affected by the instrument itself and the selected measurement methods but also greatly restricted by the engineering geological environment, rock conditions, and other factors. Because the gold mine is located below the seabed, with developed joints and fissures and strong water conductivity, the selection of measuring points needs to be more careful. All the measurement points were arranged far away from faults, rock fracture zones, and large excavations were located in the original rock stress zone (the borehole reached a depth of approximately five times the roadway span) to avoid the effect of mining disturbance. Consequently, the stress measurements represent the regional stress field.

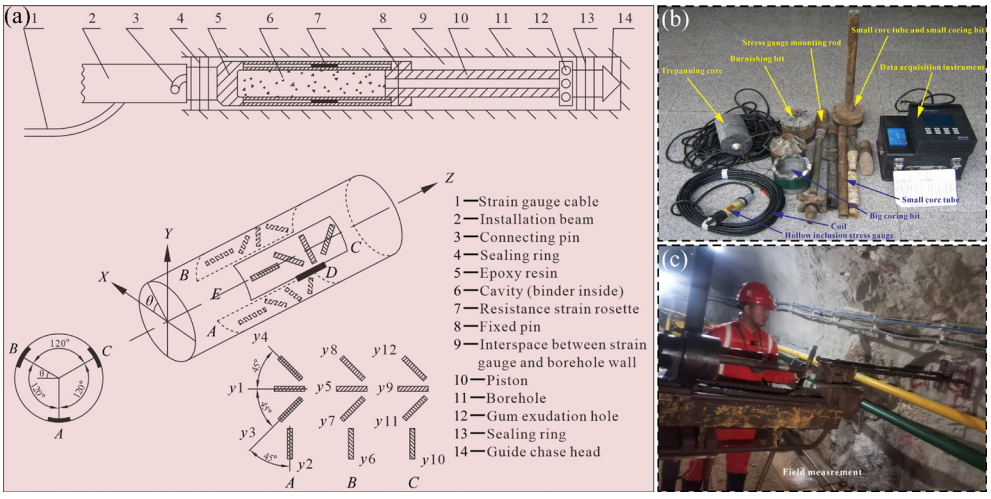

Fig. 4 Illustration of structure of improved hollow inclusion strain gauge (a) [9], overcoring equipment (b), and field measurement (c)

To obtain accurate and reliable stress measurement results, the overcoring equipment, setup, and test procedures (Fig. 4(b)) that were employed at the measurement points followed the methods suggested by the ISRM [37]. According to the basic principle of the overcoring method with a hollow inclusion strain gauge, field measurements (Fig. 4(c)) generally involve the following steps. (1) A large horizontal hole with a diameter of 130 mm is drilled perpendicularly to the roadway wall at the selected measuring point to the depth at which in situ stresses need to be determined, and then a concentric small hole with a diameter of 36 mm is drilled from the bottom of the large hole. (2) The hollow inclusion strain gauge is sent to the predetermined position in the small hole by the installation rod with the orientation device (which can eliminate the influence of environmental and human factors) and is cemented to the wall with the small hole by a special cementation system. (3) A thin-walled drill bit with a diameter of 130 mm is used to continue to extend the large hole for casing drilling so that the rock core around the small hole is separated from the surrounding rock mass to realize stress relief. (4) During the overcoring in the field, the borehole strain data and the temperature change in the measuring point measured by each strain gauge in the hollow inclusion are continuously and automatically recorded by the data acquisition instrument. All field tests were completed by skilled workers.

According to the field stress relief test results, indoor biaxial confining pressure experiments, temperature calibration test results, and the 3D stress state, including the value and orientation of the three principal stresses, in the host rock can be calculated by the following equations [34]:

$$\varepsilon_\theta = \frac{1}{E}\{(\sigma_x+\sigma_y)K_1 + 2(1-\upsilon^2)[(\sigma_y-\sigma_x)\cdot \cos 2\theta - 2\tau_{xy}\sin 2\theta]K_2 - \upsilon\sigma_z K_4\} \quad (1)$$

$$\varepsilon_z = \frac{1}{E}[\sigma_z - \upsilon(\sigma_x+\sigma_y)] \quad (2)$$

$$\gamma_{\theta z} = \frac{4}{E}(1+\upsilon)(\tau_{yz}\cos\theta - \tau_{zx}\sin\theta)K_3 \quad (3)$$

$$\varepsilon_{\pm 45^\circ} = \frac{1}{2}(\varepsilon_\theta + \varepsilon_z \pm \gamma_{\theta z}) \quad (4)$$

where ε_θ, ε_z, $\gamma_{\theta z}$, and $\varepsilon_{\pm 45^\circ}$ are the circumferential strain, axial strain, shear strain, and the strain at 45° to the axis, respectively; σ_x, σ_y, σ_z, τ_{xy}, τ_{yz}, and τ_{zx} are the six components of the original rock stresses; E and υ are the elastic modulus and Poisson's ratio, respectively; θ is the separation angle between the strain gauge and the X-axis; and K_1, K_2, K_3, and K_4 are the four correction coefficients.

Notably, the elastic modulus and Poisson's ratio of the cored rocks are two indispensable parameters that can be determined based on confining pressure experiments. These two parameters are calculated as follows [34]:

$$E = K_1(P_c/\varepsilon_\theta)\frac{2R^2}{(R^2-r^2)} \quad (5)$$

$$\upsilon = \varepsilon_\theta/\varepsilon_z \quad (6)$$

where P_c is the confining pressure, and r and R are the inner and outer radii of the core, respectively.

The complete stress tensor of each measurement point is calculated with the knowledge of the laboratory-determined final strains, and the elastic modulus and Poisson's ratio of the overcored rock. In the calculation program, the double iteration method was used. At the same time, the F test was also adopted to eliminate abnormal data to reduce the calculation error. The detailed information of the determined stress values and orientations is presented in Table 1, in which σ_1, σ_2, and σ_3 are the maximum, intermediate, and minimum principal stresses, respectively, and σ_H, σ_h, and σ_v are the corresponding maximum horizontal, minimum horizontal, and vertical principal stresses, respectively. The depth of the test sites varies from 75 to 960 m below the surface. According to the World Stress Map Quality Ranking System [38], the measured stress data can be ranked as Category B.

4.2 Anelastic strain recovery stress measurements

Additionally, to guide the design and construction of a new deep shaft in the mine area, a large number of stress measurements have been performed recently in the exploration drill holes in this area using the anelastic strain recovery method and the typical hydraulic fracturing technique [39].

The anelastic strain recovery method is a 3D stress measurement technique that has been newly developed in recent years on the basis of directional cores [40,41]. When a load is applied to a rock, the rock immediately undergoes elastic deformation and then creeps. The rock deformation recovers elastically and immediately when load is removed,

Table 1 Overcoring stress measurement results at 18 points in mine area

Point No.	Depth/m	σ_1			σ_2			σ_3			σ_h/σ_v	σ_H/σ_v	$(\sigma_H+\sigma_h)/(2\sigma_v)$	σ_H/σ_h
		Value/MPa	Direction/(°)	Dip/(°)	Value/MPa	Direction/(°)	Dip/(°)	Value/MPa	Direction/(°)	Dip/(°)				
1	75	6.01	288.50	−6.30	3.81	198.00	−4.90	2.56	250.40	82.00	1.49	2.35	1.92	1.58
2	150	7.73	280.90	−5.20	5.48	9.40	16.60	4.50	27.70	72.50	1.22	1.72	1.47	1.41
3	420	19.27	284.10	−21.30	11.05	18.50	−11.10	10.88	134.40	−65.70	1.02	1.77	1.39	1.74
4	420	19.39	120.40	−14.90	10.92	169.20	68.10	9.44	34.70	15.80	0.86	1.78	1.32	2.05
5	510	24.55	129.00	4.00	16.35	−138.00	2.00	14.49	133.00	−85.00	1.13	1.69	1.41	1.50
6	510	24.64	−111.00	3.00	15.68	155.00	82.00	15.02	161.00	−10.00	0.96	1.57	1.26	1.64
7	555	25.71	−45.00	−13.00	14.00	14.00	73.00	13.00	50.00	−20.00	0.93	1.84	1.38	1.98
8	600	28.88	103.00	1.00	16.54	10.00	76.00	14.77	13.00	−8.00	0.89	1.75	1.32	1.96
9	600	30.17	110.00	−16.00	18.83	24.00	−11.00	16.94	236.00	−70.00	1.11	1.78	1.45	1.60
10	645	29.57	112.00	−3.00	19.56	−177.00	−80.00	15.48	−156.00	−9.00	0.79	1.51	1.15	1.91
11	690	31.50	−80.00	2.00	19.08	230.00	−79.00	17.54	10.00	−10.00	0.92	1.65	1.29	1.80
12	690	29.77	−83.00	4.00	20.84	−8.00	−74.00	19.63	8.00	15.00	0.94	1.43	1.19	1.52
13	750	33.22	119.00	−10.00	19.93	−89.00	−82.00	17.10	208.00	−8.00	0.85	1.69	1.27	1.99
14	750	32.78	105.60	−0.59	19.6	18.70	79.20	16.68	15.50	−10.80	0.86	1.64	1.25	1.92
15	780	30.72	133.30	−14.90	26.41	−135.60	−4.17	18.09	149.7	74.50	1.46	1.70	1.58	1.16
16	795	48.93	164.09	3.00	23.15	74.41	−5.97	21.66	47.22	83.29	1.07	2.26	1.66	2.11
17	825	46.95	40.06	3.84	28.88	−49.55	−5.77	26.49	−83.43	83.06	1.09	1.77	1.43	1.63
18	960	41.63	145.30	−10.30	26.79	165.50	60.30	25.42	200.20	−6.21	0.95	1.55	1.25	1.64

and with increasing time, the inelastic strain recovers slowly. Therefore, the in situ stress magnitude can be converted by measuring the inelastic strain recovery of directional cores, and the stress orientation of the core can be determined by paleomagnetic techniques or image logs [42]. Compared with other core-based methods for stress measurement, the anelastic strain recovery technique has a relatively perfect theoretical basis, and this method uses drill cores for field measurements, thus maintaining the approximate in situ state of the cores.

The initial two-dimensional anelastic strain recovery method was applied to the in situ stress measurements of oil and gas fields and was further developed into a three-dimensional approach by MATSUKI and TAKEUCHI [43]. Based on the assumption that the rock is homogeneous, isotropic, and linearly viscoelastic, the principal strain direction calculated from the inelastic recovery strain in at least six independent directions measured by this method is the principal stress direction. The relationship between the principal stress and inelastic recovery strain can be expressed as [44]

$$\varepsilon_{\mathrm{a}}(t)=\frac{1}{3}[(3l^2-1)\sigma_x+(3m^2-1)\sigma_y+(3n^2-1)\sigma_z+6lm\tau_{xy}+6mn\tau_{yz}+6nl\tau_{zx}]\mathrm{Jas}(t)+(\sigma_{\mathrm{m}}-P_0)\mathrm{Jav}(t)+\alpha_{\mathrm{T}}\Delta T(t) \quad (7)$$

where $\varepsilon_{\mathrm{a}}(t)$ is the inelastic recovery strain; P_0 is the pore pressure; l, m, and n are the direction cosines of the strain axis; σ_{m} is the average normal stress; α_{T} is the coefficient of linear thermal expansion; $\Delta T(t)$ is the temperature change during the measurement; and Jas(t) and Jav(t) are the inelastic strain recovery compliances of shear and volume deformation modes, respectively.

The magnitude of the principal stress (σ_i) can be calculated as

$$\sigma_i=e_i(t)/\mathrm{Jas}(t)+[e_{\mathrm{m}}(t)-\sigma_{\mathrm{T}}\Delta T(t)]/\mathrm{Jav}(t)+P_0 \quad (8)$$

where $e_{\mathrm{i}}(t)$ is the inelastic deviatoric strain, σ_{T} is the tensile strength and $e_{\mathrm{m}}(t)$ is the average normal strain.

More details of the test process and data

processing of this method can be found in Ref. [40]. According to the test record curves of the inelastic strain recovery method collected from eight core samples with different burial depths in the mine area, the in situ stresses of these eight core samples were inversed [39], and the calculation results are shown in Table 2. The measurement depths vary from 862 to 1888 m, and the stress data quality can be ranked as Category B [38].

4.3 Hydraulic fracturing stress measurements

The hydraulic fracturing technique is also a popular stress measurement method recommended by the ISRM [18]. After the first application in oil fields to increase production, this method has been greatly improved for decades, both theoretically and technically. Compared with the overcoring technique, the hydraulic fracturing technique can reveal stress information at greater depths. The hydraulic fracturing technique involves isolating a short section of the wellbore between rubber packers and increasing the hydraulic pressure in the isolated interval until a small tensile fracture is induced, usually parallel to the maximum horizontal principal stress orientation [45]. According to the principles of elasticity and fracture mechanics, the fracture surface trend of the fracturing section caused by hydraulic fracturing is the maximum horizontal principal stress orientation. Indeed, typical hydraulic fracturing is a two-dimensional stress measurement method with the assumption that one principal stress component is vertical, which is suitable only for determining the maximum and minimum horizontal stresses.

The directions of the principal stresses in the plane perpendicular to the drilling axis are identified based on the azimuth of the induced hydraulic fracture, which can be obtained and yielded by running an oriented impression packer or borehole image logs over the fractured section [46,47]. The stress magnitudes are determined based on the borehole pressures that open and close the hydro-fractures several times (normally 4−5 cycles). According to the measured original data, the key stress-related test interval pressures (i.e., the breakdown pressure P_b, shut-in pressure P_s, and reopening pressure P_r), the rock pore pressure P_0 (which is equal to the hydrostatic pressure), and the in situ tensile strength σ_T of the tested rock can be obtained. Then, the maximum (σ_H) and minimum (σ_h) horizontal principal stresses are determined using the relevant formulas (Eqs. (9) and (10)), with these measured parameters. The key to calculating in situ stresses from hydraulic fracturing results is to correctly determine the values of P_s and P_r. At present, there is no unified standard method to determine P_s and P_r. Several approaches, such as the inflection point and exponential pressure-decay methods, have been suggested to determine P_s [48]. Usually, a combination of two or more methods is needed. For the determination of P_r, one practicable method is that P_r can be obtained by comparing the first pressurization cycle with the second (or third, fourth, etc.) pressurization cycle. The pressure–time curves of the second pressurization cycle and the first pressurization cycle overlap, and then a point where the second pressurization cycle curve deviates from the first pressurization cycle curve is selected as the fracture reopening point, and the pressure at this point is designated P_r. In addition,

Table 2 Anelastic strain recovery stress measurement results in mine area [39]

Point No.	Depth/ m	σ_H			σ_h			σ_v			σ_h/σ_v	σ_H/σ_v	$(\sigma_H+\sigma_h)/(2\sigma_v)$	σ_H/σ_h
		Value/ MPa	Direction/ (°)	Dip/ (°)	Value/ MPa	Direction/ (°)	Dip/ (°)	Value/ MPa	Direction/ (°)	Dip/ (°)				
1	862	31.6	305	2	23.5	35.2	5	22.4	13.3	−84.6	1.05	1.41	1.23	1.34
2	922	32.4	309.3	1.5	25.9	39.2	−3	24.0	−65.8	−86.6	1.08	1.35	1.21	1.25
3	1162	41.3	306.3	−3	33.2	36.2	2.5	30.2	86.4	−86.1	1.10	1.37	1.23	1.24
4	1267	45.9	302.3	1.5	32.5	32.3	0	33.0	−57.7	−88.5	0.98	1.39	1.19	1.41
5	1405	47.6	292.7	1	36.1	22.7	2	36.5	−3.9	−87.8	0.99	1.30	1.15	1.32
6	1500	51.5	294.7	1.5	38.1	24.7	1.5	39.0	−20.3	−87.9	0.98	1.32	1.15	1.35
7	1687	60.4	296.7	1.5	41.8	26.7	1.5	43.8	−18.3	−87.9	0.95	1.38	1.17	1.44
8	1888	67.3	298.3	3	48.4	28.4	1.5	49.1	−35.1	−86.6	0.99	1.37	1.18	1.39

the vertical (σ_v) principal stress is estimated from the weight of overlying strata (Eq. (11)).

$$\sigma_H=3P_s-P_r-P_0 \quad (9)$$

$$\sigma_h=P_s \quad (10)$$

$$\sigma_v=\gamma H \quad (11)$$

where γ is the mean rock density and is assumed to be 2650 kg/m^3 , and H is the depth.

The selected fractured rocks in the mine area are almost intact and lack obvious cracks, thus ensuring the integrity of the data in the hydraulic fracturing test process. As a result, 23 fracturing sections were successfully tested, and the relationship between pressure and time was recorded synchronously [39]. Three test sections with depths of 509.35, 1097.5, and 1512.5 m were selected for directional calibration using an oriented impression packer, thus determining the maximum horizontal principal stress directions of these three fractured sections. The 23 sets of hydraulic fracturing stress measurement results varying from 357.76 to 1899.00 m are listed in Table 3 [39]. The hydraulic fracturing data quality can be ranked as Category C [38]. The anelastic strain recovery and hydraulic fracturing measurements compensate for the lack of stress data in the deep part (>1000 m) of the mine area.

Finally, a total of 49 groups of stress data, including these three different types of data, are employed to characterize the current stress tensor in the mine area to understand the regional present-day stress state and its relationship to tectonization. Notably, these measurement campaigns were performed as a part of field investigations to guide

Table 3 Hydraulic fracturing stress measurement results in mine area [39]

Point No.	Depth/ m	Pressure parameters/MPa					Principal stress/MPa			σ_H direction	σ_h/σ_v	σ_H/σ_v	$(\sigma_H+\sigma_h)/(2\sigma_v)$	σ_H/σ_h
		P_b	P_r	P_s	P_0	σ_T	σ_H	σ_h	σ_v					
1	357.76	20.02	15.54	11.73	3.51	4.48	23.16	15.24	9.47	−	1.61	2.45	2.03	1.52
2	431.09	24.57	15.78	11.85	4.22	8.79	23.99	16.08	11.41	−	1.41	2.10	1.76	1.49
3	509.35	25.15	20.29	13.44	4.99	4.86	25.02	18.43	13.48	N55.5°W	1.37	1.86	1.61	1.36
4	608.26	25.16	18.82	14.35	5.96	6.34	30.20	20.31	16.39	−	1.24	1.84	1.54	1.49
5	665.33	24.34	21.39	14.75	6.52	2.95	29.37	21.27	17.60	−	1.21	1.67	1.44	1.38
6	881.70	30.22	23.09	16.29	8.64	7.14	34.42	24.93	23.33	−	1.07	1.48	1.27	1.38
7	957.10	25.86	22.54	16.57	9.38	3.33	36.56	25.95	25.32	−	1.02	1.44	1.23	1.41
8	1010.50	23.06	19.19	16.48	9.90	3.87	40.14	26.38	27.23	−	0.97	1.47	1.22	1.52
9	1097.50	30.43	25.72	20.19	10.76	4.71	45.62	30.95	29.04	N60.4°W	1.07	1.57	1.32	1.47
10	1166.41	34.84	25.72	20.50	11.43	8.90	46.99	31.93	30.86	−	1.03	1.52	1.28	1.47
11	1220.40	34.40	25.31	20.44	11.96	9.09	47.96	32.40	32.29	−	1.00	1.49	1.24	1.48
12	1275.80	32.79	23.63	19.52	12.50	9.16	47.43	32.02	34.38	−	0.93	1.38	1.16	1.48
13	1350.00	29.30	21.84	18.62	13.23	7.47	47.25	31.85	35.72	−	0.89	1.32	1.11	1.48
14	1408.00	28.02	23.36	19.32	13.80	4.66	48.40	33.12	37.26	−	0.89	1.30	1.09	1.46
15	1473.18	31.93	24.09	20.59	14.44	7.85	52.12	35.03	38.98	−	0.90	1.34	1.12	1.49
16	1512.50	31.01	24.98	20.75	14.82	6.04	52.11	35.58	40.02	N58.4°W	0.89	1.30	1.10	1.46
17	1594.60	31.82	26.59	22.12	15.63	5.23	55.40	37.75	42.19	−	0.89	1.31	1.10	1.47
18	1643.63	38.98	29.43	24.70	16.11	9.55	60.79	40.81	44.30	−	0.92	1.37	1.15	1.49
19	1689.50	37.83	28.31	24.46	16.56	9.52	61.63	41.02	44.70	−	0.92	1.38	1.15	1.50
20	1756.80	34.89	30.65	26.39	17.22	4.24	65.72	43.60	46.48	−	0.94	1.41	1.18	1.51
21	1792.70	32.69	27.70	24.83	17.57	4.99	64.37	42.40	47.43	−	0.89	1.36	1.13	1.52
22	1839.00	37.35	28.73	25.43	18.02	8.62	65.58	43.45	49.56	−	0.88	1.32	1.10	1.51
23	1899.00	42.47	33.10	28.45	18.61	9.37	70.86	47.06	50.25	−	0.94	1.41	1.17	1.51

mining activities. More importantly, the obtained reliable and various stress measurements can also be used to yield a picture of the general state of regional stresses and describe the regional stress pattern and its inhomogeneity. This is conducive to revealing more details of the tectonic stress field and improving the geological interpretation of the study area and surrounding districts.

5 Present-day stress field

5.1 In situ stress magnitudes

For overcoring stress measurements (Table 1), the two principal stresses at each measurement point are nearly horizontal, the angles between the two principal stress directions and the horizontal plane are generally less than 10°, and a few larger angles, which are called the maximum (σ_H) and minimum (σ_h) horizontal principal stresses, respectively, do not exceed 21.3°. The third principal stress lies in an approximately vertical direction, with a vertical angle that is not larger than 30°, which is regarded as the vertical (σ_v) principal stress. This regularity is much more remarkable in plains districts than in mountainous districts. At all test sites, the maximum horizontal principal stress is far higher than the vertical component. This result provides strong evidence that the stress field in the mine area is governed by horizontal tectonic stresses, which are all compressive stresses. In other words, the horizontal stress condition in this area is predominantly tectonically driven and not just gravity-induced. This finding has been observed in many other regions [46]. The tunnel deformation failure investigation and the engineering geological survey in the mine area suggest that horizontal tectonic stress is dominant in this area, so the measured stress results are identical to those of the structural investigation and the focal mechanism solutions.

The stress measurements available in the mine area suggest that the stress conditions in this area appear to favor thrust ($\sigma_H>\sigma_h>\sigma_v$) and strike-slip ($\sigma_H>\sigma_v>\sigma_h$) faulting regimes within the tested depth intervals. Specifically, the order of $\sigma_H>\sigma_h>\sigma_v$ appears at 21 measurement sites, accounting for 42.86% of the total sites, and the order of $\sigma_H>\sigma_v>\sigma_h$ is present at 28 measurement sites, accounting for 57.14% of the total sites; both show a random distribution with depth. Given that the depths of these measurements are less than 2000 m, it is not surprising that such a phenomenon appears, as this phenomenon has been reported by other researchers [49]. Nevertheless, at depths less than 1000 m, 17 of 27 test sites are characterized by $\sigma_H>\sigma_h>\sigma_v$, and 18 of 22 test sites are characterized by $\sigma_H>\sigma_v>\sigma_h$ at depths higher than 1000 m. Overall, with increasing depth, the vertical principal stress tends to change from the minimum to the intermediate principal stress, that is, the stress state transitions from the shallow thrust faulting regime to a regime favoring strike-slip faulting at depth. This is a typical feature of the stress regime in this mine area. In fact, similar stress conditions changing from a thrust faulting regime at shallow depths to a strike-slip faulting regime and sometimes a normal faulting regime ($\sigma_v>\sigma_H>\sigma_h$) at deeper depths have been observed in other locations, such as northern Switzerland and the Perth Basin of Western Australia [15]. This transformation highlights the fact that "depth" is a key factor in studying the stress state, and the stress state at different depths is not necessarily constant. At the same time, we should be especially careful when using the surface geological structure as the only source of stress state information of the geomechanical model because surface faulting may not directly indicate a deeper stress state.

In addition, in the 49 measuring points, 47 σ_H magnitudes are greater than 18 MPa and even exceed 30 MPa, accounting for 95.92% of the total measuring points. Hence, the stress state of the mine area is at a high stress level overall based on the assessment standard of the stress level of the engineering rock mass [50]. In addition, compared with the tectonic stress field of the entire North China region [51], the in situ stress of this mine area is also at a high stress level.

Figure 5 illustrates the individual measurement results given in Tables 1, 2, and 3 in the form of σ_H, σ_h, and σ_v as a function of depth. The three principal stresses all increase approximately linearly with depth, despite certain scatter in the stress data. Thus, linear regressions are reasonable representations of the σ_H, σ_h, and σ_v variations with depth H, and the best-fit linear relationships can be expressed as

$$\sigma_H=0.0306H+9.1659,\ R^2=0.9398 \quad (12)$$

$$\sigma_h=0.0223H+4.1118,\ R^2=0.9575 \quad (13)$$

$$\sigma_v=0.0260H+0.7749,\ R^2=0.9935 \quad (14)$$

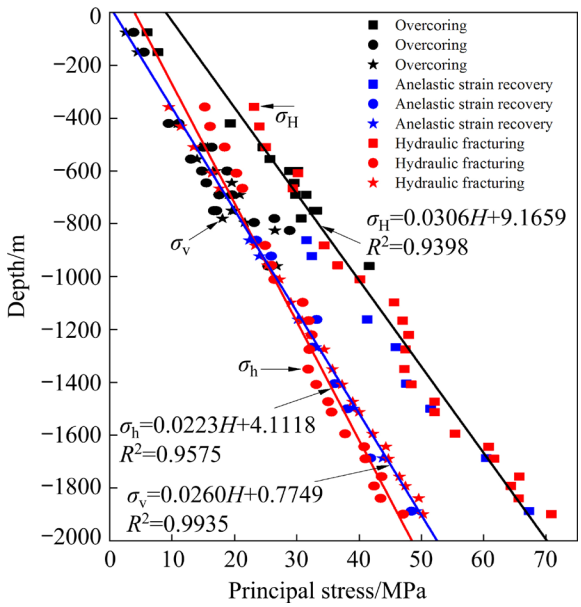

Fig. 5 Variations of σ_H, σ_h, and σ_v with depth

The regression lines between the three principal stresses and depth are plotted in Fig. 5. Although three stress measurement methods are used, the linear correlation coefficients (R^2) of the obtained σ_H, σ_h, and σ_v values are 0.9398, 0.9575, and 0.9935, respectively, signifying that the degree of linear correlation is quite high and that the increased pattern of the stress magnitude within the tested depth intervals in the mine area has not changed significantly. Compared with the deep stress data, the shallow stress data are slightly scattered, which may be induced by the uneven distribution of in situ stress due to the terrain effect and influence of historical geological structures. The regression coefficient of 0.026 in the regression equation of σ_v is very close to the average bulk density of overlying strata 0.026×10^3–0.027×10^3 kN/m^3, which reflects the fact that σ_v is generally equal to or slightly smaller than the weight of the overburden. Theoretically, according to the linear regression curves, firstly, σ_v is smaller than σ_h and then larger than σ_h when the depth reaches 902 m because the growth rate of σ_v is greater than that of σ_h. The growth rates of σ_h and σ_v are much smaller than that of σ_H (0.0306 MPa/m). Consequently, within the tested depths, σ_h and σ_v are smaller than σ_H, and if this variation with depth exhibited in Fig. 5 is extrapolated to deeper depths, the differences among σ_H, σ_h and σ_v seem to increase with increasing depth.

The individual constant terms in the linear regression equations of σ_H and σ_h are larger than that in the linear regression equation of σ_v, which indicates that significant horizontal tectonic stress still exists near the mine area surface. Furthermore, linear growth of the three principal stresses means that there is a great effect of high in situ stress in the deep part of the gold mine. Typically, the high in situ stress creates favorable conditions for high energy accumulation in the rock mass and the occurrence of dynamic disasters, such as rock bursts. Because the mining depth of the gold mine exceeds 1000 m, great in situ stress will be encountered in the mining process. To ensure the safety of mining, reasonable support and reinforcement measures must be taken, and all kinds of ground pressure activities and dynamic disasters caused by high stress should be monitored and controlled during the whole process of mining. On the other hand, based on crustal structural analysis, early estimations indicated that the variations in horizontal principal stresses with depth may change significantly after the depth exceeds 1000 m, that is, the increase rate of horizontal principal stresses will slow down [52]. The stress measurements at great depths in recent years, including the measurements in the study area, cannot prove this estimation. To rigorously evaluate at what depth a turning point in the growth rate of the principal horizontal stress occurs, more and deeper in situ stress measurement data are needed.

The abovementioned in situ stress distribution pattern is basically consistent with the deformation and failure pattern of roadways in the gold mine. There are few problems with shallow mining at this mine, but many serious roadway deformations and failures occur in deep mining, which is the result of the increase in the in situ stress with increasing depth. The investigation results of roadways at depths of 870 and 915 m show that the main forms of deformation and failure are local spalling, falling roofs, obvious roadway section reduction, serious deformation of supporting structures, and slight rock bursts. All these phenomena further indicate that a large horizontal tectonic stress exists in the mine area. Hence, reasonable and effective measures must be taken to control the effect caused by in situ stress and maintain the stability of underground mining structures, such as stopes and roadways.

Moreover, the ratio between horizontal principal stresses and the ratio of horizontal to vertical principal stress are of great significance, reflecting the key characteristics of the stress distribution. At all points, the ratios of σ_h to σ_v (σ_h/σ_v), σ_H to σ_v (σ_H/σ_v), average horizontal principal stress to vertical principal stress ($(\sigma_H+\sigma_h)/(2\sigma_v)$), and σ_H to σ_h (σ_H/σ_h) are calculated and plotted as a function of depth in Fig. 6. σ_h/σ_v, σ_H/σ_v, and $(\sigma_H+\sigma_h)/(2\sigma_v)$ decrease nonlinearly with increasing depth, and their relationships with depth are fitted in the form of hyperbolas, as provided in Figs. 6(a), (b), and (c), respectively. As the depth increases, the three coefficients seem to approach the constants of 0.96, 1.45, and 1.20, respectively. Furthermore, σ_h/σ_v varies from 0.79 to 1.61, with an average of 1.03 (Fig. 6(a)), and the maximum and minimum values of σ_H/σ_v are 2.45 and 1.30, respectively, with an average of 1.58 (Fig. 6(b)). The observed ranges of σ_h/σ_v and σ_H/σ_v are similar to those obtained from less than 2000 m in more than 30 countries worldwide [53]. Based on elasticity theory, the width/height ratio of the roadway cross-section should be consistent with the ratio of the two principal stresses acting on the cross-section as much as possible in future roadway designs of the gold mine to reach a state of uniform isostatic stress, which is beneficial to improving the stress distribution of the surrounding rock and reducing the deformation and failure of the roadway.

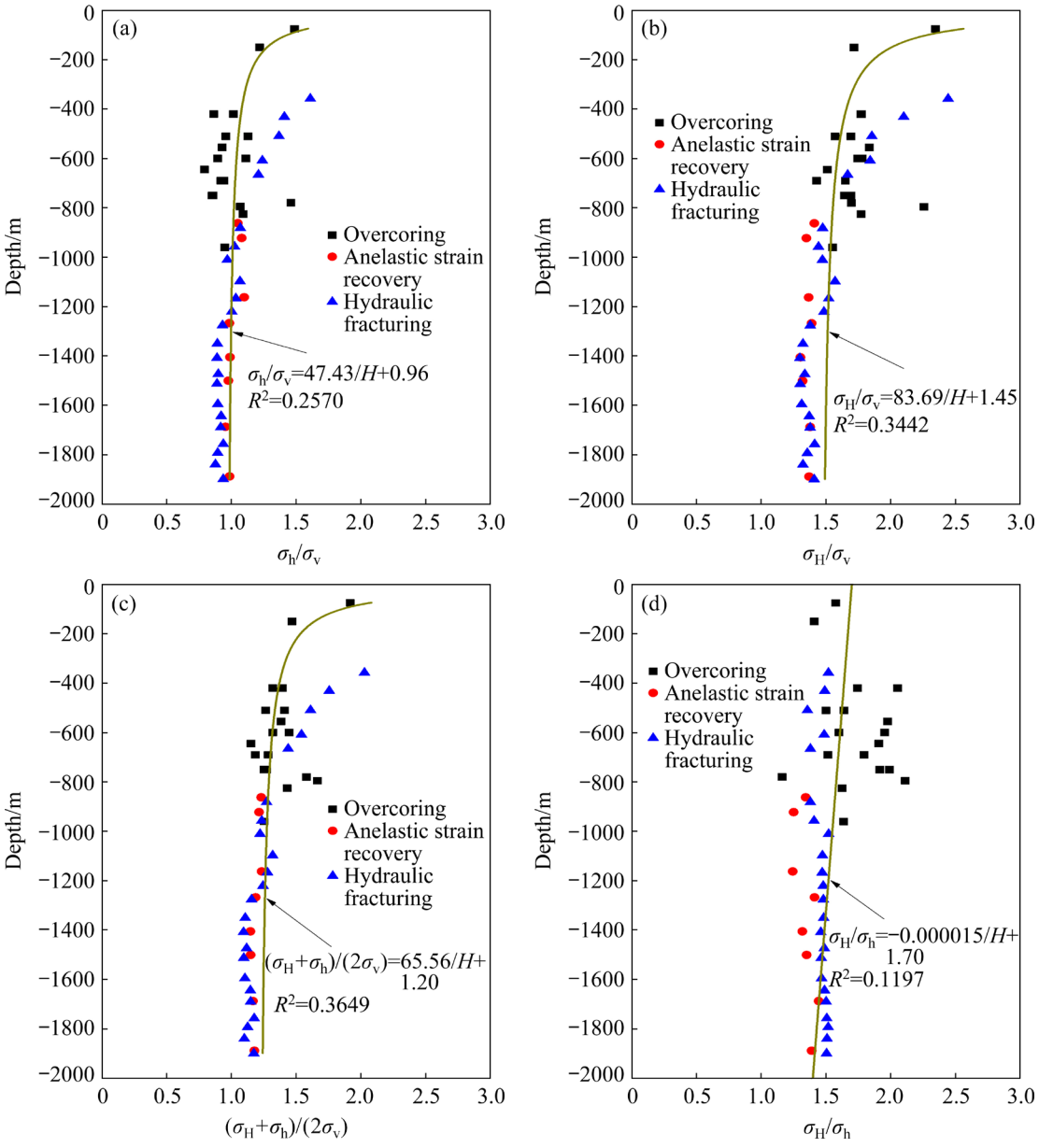

Fig. 6 Variations of stress ratio with depth: (a) σ_h/σ_v; (b) σ_H/σ_v; (c) $(\sigma_H+\sigma_h)/(2\sigma_v)$; (d) σ_H/σ_h

$(\sigma_H+\sigma_h)/(2\sigma_v)$ is basically stable in the whole mine area, mostly ranging from 1.09 to 1.50 and averaging 1.31 (Fig. 6(c)). According to the macroscopic classification of the original rock stress field [54], the in situ stress field is a geodynamic stress field within the measured depths in the mine area but tends to gradually transition to a quasi-hydrostatic pressure field with increasing depth. Notably, as the burial depth of the determined stress data in this study is less than 2000 m, it is not known whether there is hydrostatic pressure in the deep part of the mine area, and a large body of stress data in the deeper part is needed for further study. In addition, the relationship between the coefficient and depth in this area is similar to the overall variation characteristics of the relationship curve summarized by BROWN and HOEK [55] using the compiled stress data worldwide, but there are some differences in values that are close to the inner envelope of the Hoek–Brown curve. The reason is that the Hoek–Brown curve is a summary of the global stress distribution, and the stress distribution is very regional, which is not only related to the lithology of a specific region but also greatly influenced by regional tectonic movement. Because different regions in the world are greatly influenced by historical and present tectonic movements, the characteristics of tectonic stress fields are also considerably different, which is one of the reasons for the large differences between the Hoek–Brown inner and outer envelope curves. The distribution features of the stress field in this region, to a certain extent, reflect the characteristics of lithology and historical and contemporary tectonic movements. The stress measurement results imply that although the changing trend of in situ stress is similar to the Hoek–Brown curve, the in situ stress field in this area has its characteristics, and the test results of other industries and even other metal mine areas cannot be applied uncritically.

σ_H/σ_h reflects the characteristics of horizontal tectonic stress. This coefficient is between 1.16 and 2.11, with an average of 1.55 (Fig. 6(d)). Apparently, the influence of horizontal principal stresses on underground excavations has obvious directionality. σ_H/σ_h has no significant correlation with depth, and its relationship with depth is fitted in the form of a linear curve, which can be used to roughly express the overall trend. Moreover, the fluctuation range of the coefficient in the shallow zone is wider than that in the deep zone, indicating that the stress distribution in the same plane in the deep zone tends to be more uniform than that in the shallow zone. The difference in the two horizontal principal stresses in the same plane reflects the instability degree of the rock mass, and a large difference easily causes deformation and failure of the surrounding rock. Based on Mohr's strength theory, the maximum shear stress can be regarded as $(\sigma_H-\sigma_h)/2$, and the failure of the surrounding rock in mines is usually induced by the shear stress. The difference between σ_H and σ_h at almost all measuring points in the mine area is large, implying that the shear stress is high in the horizontal plane. This is a characteristic of the in situ stress distribution in this region, which is unfavorable to the stability of the underground mining system. On the other hand, as the shear stress exceeds the shear strength of the rock mass, the rock mass breaks, which provides favorable stress conditions for the formation of faults, joints, and other structures. This is one of the mechanical reasons for the relatively developed and densely distributed faults and joints in the mine area.

5.2 In situ stress direction

The σ_H direction is a crucial component of stress tensors and has received extensive attention in the mining industry. The σ_H directions at 18 measuring points (except two points) yielded from the overcoring method are similar, ranging from N30°W to N90°W, with an average of 110.9° (i.e., N69.1°W), as shown in the rose diagram in Fig. 7(a). The σ_H directions at the eight test sites measured by the anelastic strain recovery method are 305°, 309.3°, 306.3°, 302.3°, 292.7°, 294.7°, 296.7°, and 298.3°, with an average of 300.7° (i.e., 120.7°, N59.3°W) (Fig. 7(b)). Moreover, the σ_H directions in the three test sections determined by the hydraulic fracturing method are N55.5°W, N60.4°W, and N58.4°W, with an average of 121.9° (i.e., N58.1°W) (Fig. 7(c)). Obviously, the stress measurements provided by the three different methods agree well.

Figure 8 shows the directional characteristics of σ_H obtained by the three methods in a depth profile and map view in the mine area. A common

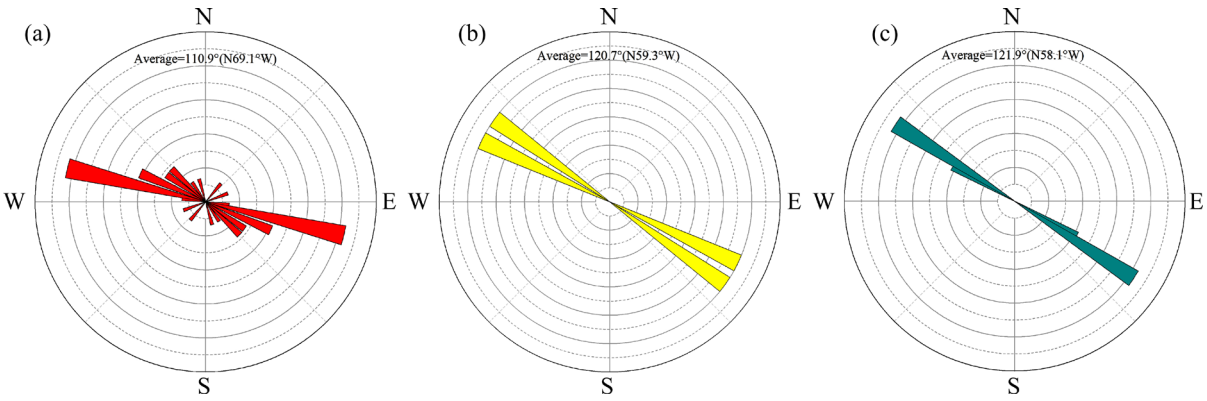

Fig. 7 σ_H direction revealed by three stress measurement methods: (a) Overcoring; (b) Anelastic strain recovery; (c) Hydraulic fracturing

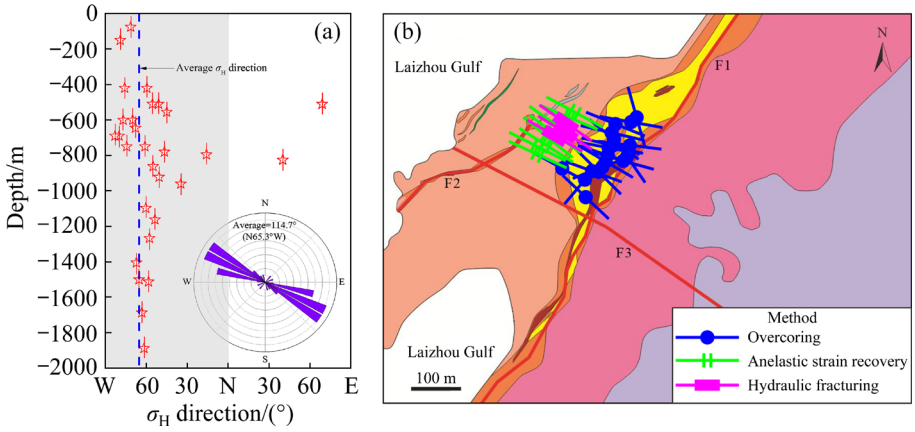

Fig. 8 σ_H direction in depth profile (a) and map view (b) in mine area

denominator appears to exist among the obtained stress direction data regardless of depth, indicating a consistent WNW–ESE or approximately E−W orientation, which reflects that the action of principal compressive stress at different depths of the crust is obviously consistent. This result concurs well with the direction of the regional tectonic stress field reflected by neotectonic movement and modern focal mechanism solutions (Fig. 3(b)), which implies that the stress measurements in this mine are reliable and show the same type of stress pattern. Typically, the famous deep-seated Tan–Lu fault zone on the west side of the mine area is a currently active dextral strike-slip zone, and its movement pattern agrees fairly well with the expected action of the measured stress direction. In addition, the maximum principal stress orientations derived from overcoring stress measurements in the Linglong and Xincheng gold mines [11,14] adjacent to this gold mine, as well as hydraulic fracturing stress measurements in an underground engineering area [56] far from the gold mine in the Jiaodong Peninsula are in good agreement with those determined in the study area.

The World Stress Map [38], which is highly recognized worldwide, adopts the strict quality standards and mainly shows the strike-slip faulting conditions according to the earthquake focal mechanism solutions around the mine area (Fig. 9) [5]. Moreover, according to various stress indicators, such as borehole breakout analyses, in the vicinity of the mine area, including inland and sea areas, the σ_H direction is generally WNW–ESE to E−W (Fig. 9). Remarkably, these orientations provided by the World Stress Map are practically in line with those determined in this study. In addition, under the driving plate conditions, the crust deforms and produces a horizontal compressive stress field in the crust. The current stress pattern of the mine area is inevitably influenced and controlled by the activities of the surrounding plates (i.e., the Indian, Pacific, and Philippine plates) as

well as the interaction of terrestrial blocks (such as the Northwestern China block and Qinghai−Tibet block) [51,57]. It is well known that the pattern of the σ_H direction is a reliable indicator of the dynamic background. The determined predominant σ_H direction in the study area indicates that the driving force of the area is probably composed of the nearly E−W subduction of the Pacific plate and NW compression of the Philippine plate. Notably, other plates or blocks also play a certain role in generating the modern tectonic stress model in the study area.

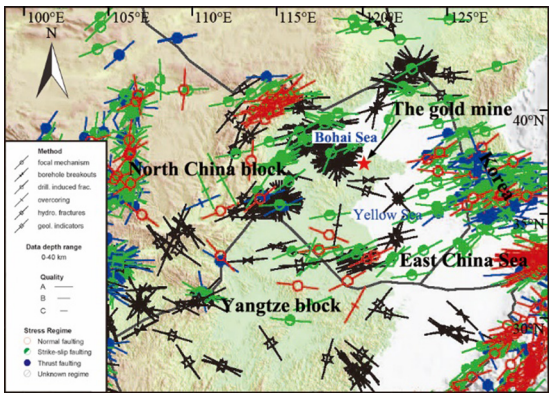

Fig. 9 Maximum horizontal stress directions indicated by World Stress Map (after HEIDBACH et al [5])

In summary, these results reinforce the WNW–ESE or approximately E−W orientation observed in this area. Consequently, we herein speculate that the stress field is significantly influenced by the prevailing WNW-trending tectonic compressive stress, which represents regional stress conditions in and around the mine area. It is worth emphasizing that at some measuring points at the same depth (i.e., in the same plane), the stress magnitude and orientation have certain changes in different positions, but there are no sudden changes, which indicates that the stress field of the mine area is relatively uniform. Moreover, due to the limitation of the test depth, the stress measurement results discussed in this study may not fully represent the tectonic stress state in this area. However, the stress information can at least indicate the relative spatial variation in the stress state.

6 Relationship between stress field and tectonization

Geological structures are structural traces preserved by the deformation and failure of crustal rocks caused by tectonic stress. Geological structures formed under different stress conditions are often different, and thus, geological structures can reflect the tectonic stress states to a certain extent when they are formed [11]. The existing form of most geological structures is regarded as the consequence of multiple tectonic activities. The tectonic movements in different stages have varying effects on the tectonic stress field, resulting in a very complicated relationship between geological structures and the tectonic stress field. Therefore, the relationship can be deeply understood by studying the tectonic evolution stages, sequential formation relations, and the characteristics of geological structures in the mine area.

6.1 Geological evolution

As previously mentioned, the mine area has undergone Indosinian, Yanshan, and Himalayan movements [20]. Since the Indosinian period, the stress field in North China has undergone many transformations under the collision and splicing of the Yangtze plate and North China plate as well as the westward subduction of the Pacific plate, thereby controlling the generation and evolution of regional geological structures. The Indosinian period was a turning period when the North China plate began to disintegrate and deform strongly and the paleogeography and paleotectonic framework changed dramatically. Indosinian movement caused obvious folding, uplift, and fault movement in the strata in the Jiaodong Peninsula before the Paleozoic, thereby forming an anticline structure mainly in the E−W direction accompanied by relatively developed NE-oriented compressional-torsional faults and poorly developed NW-oriented tensional-torsional faults near the mine area. The energy source of the Indosinian movement was the collision between the North China plate and Yangtze plate, which caused a large NE–SW compressional force [58]. Hence, in this period, the maximum principal compressive stress of the mine area was along the NE–SW direction (Fig. 10(a)), which was mainly pushed from SW to NE. This was the first-stage tectonic stress field in this area since the Mesozoic.

The Yanshanian was the intensest period in geological history for tectonic deformation and magmatic activity in the North China plate. Due to

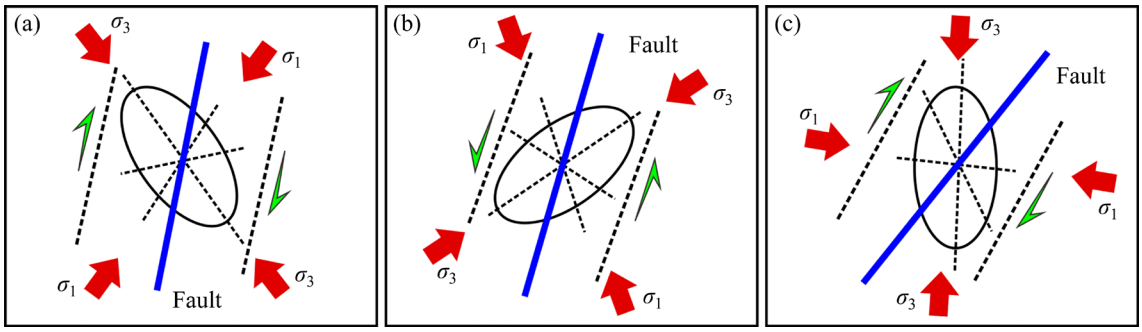

Fig. 10 Schematic diagrams of stress field characteristics corresponding to different tectonic activity evolution stages: (a) First stage; (b) Second stage; (c) Third stage

the dominant role of the northward movement of the Pacific plate, a regional sinistral coupled stress field was formed, which produced a sinistral torsion with the near N−S orientation of the mine area. The maximum compressive stress orientation across this area was nearly NW–SE (Fig. 10(b)), which was the second stage tectonic stress field, causing the faults formed in the first stage to have sinistral torsion. The original tensional and torsional activities of NE-trending faults transitioned into compressional and torsional activities, and the original compressional and torsional activities of NW-trending faults became tensional and torsional activities. During this geological period, the ENE-oriented Sanshandao–Cangshang fault zone and NW-oriented Sanshandao–Sanyuan fault in the mine area were formed and developed in this tectonic system transformation environment [20]; the Sanshandao–Cangshang fault zone had the geological characteristics of a compressive structural plane, while the Sanshandao–Sanyuan fault was a typical tensile structural plane. In addition, Linglong bedrock was also believed to have been caused by the upward emplacement of magma generated from partial crustal melting under the NW–SE compressional background in this period along with the branch fractures of the gently inclined Tan–Lu fault zone [59].

During the Himalayan movement period, the Indian plate collided strongly with Eurasia, and the effect of such collision was delivered to North China, including the mine area, to the northeast of the Qinghai−Tibet Plateau. Under the extrusion of the Indian plate along a NNE orientation, a regional dextral coupled stress field in the nearly NE direction was formed in the mine area, and the maximum principal stress direction further developed in a nearly E−W direction in this area (Fig. 10(c)), which was the third-stage tectonic stress field. Subject to this stress field, the rock mass in the ore-bearing alteration zone cemented by diagenesis experienced a new tectonic fracture. The regional nearly E−W tectonic stress field was affected by the inheritance, accommodation, and combination of the geological structures in the mine area and exhibited NE–SW compression and torsion in the area, causing dextral shear failure on the hanging wall of the Sanshandao–Cangshang fault zone. Moreover, the representative NE-striking Tan–Lu fault zone in the western mine area experienced dextral translation under the action of a nearly E−W-directed tectonic stress field. Moreover, controlled by the stress field, the Sanshandao–Sanyuan fault experienced sinistral compressional and torsional activity, thereby dislocating the Sanshandao–Cangshang fault zone. In addition, large-scale differential uplifts have occurred in this area, and neotectonic movements are relatively strong and continue into modern times.

In conclusion, the new and old tectonic systems in the mine area are closely linked. That is, the new tectonic system has inherited the old tectonic system and simultaneously shows new creative functions, producing new structural traces. Field stress measurements and theoretical studies in recent years have shown that the maximum principal compressive stress orientation primarily depends on the contemporary tectonic stress field and has no direct or inevitable connection with the tectonic stress field throughout geological history. Only when the contemporary stress field inherits the early stress field and evolves further or is well coupled with a certain historical stress field orientation can the present-day stress field

orientation be linked with the geological structural elements. The maximum principal compressive stress orientation varies from NE−SW in the first stage of tectonism to NW−SE in the second stage and finally gradually becomes nearly E−W in the third stage. Therefore, the crustal stress field is unstable but has relative stability, which is a function of time and space. According to the focal mechanism data and stress measurement results, the maximum principal stress orientations of most measurement points are mainly located in the nearly E−W and partly in the NW−SE orientations, which concurs with the earlier analysis of the tectonic stress field orientations in the second and third stages, implying that the contemporary stress conditions basically inherited the third-stage tectonic stress field while partially retaining features of the tectonic stress field in the second stage and eventually developed into a tectonic stress field controlled by approximate E−W extrusion. This further suggests that the stress direction affecting the current major structural activities of this region is in nearly the E−W direction.

6.2 Geological structural analysis

Geological tectonic lines or structural traces are indicators of the tectonic stress field. The Sanshandao–Cangshang fault zone and its adjacent Jiaojia fault zone and Zhao–Ping fault zone control the occurrence of the vast majority of superlarge and large deposits on the northwestern Jiaodong Peninsula. These three fault zones are the products of many tectonic movements since the Mesozoic and are part of the same sequence and fault grade system. Under the action of the NW–SE lateral force, the dips of these fault zones are opposite, and the lateral pressures were transferred by the Linglong and Guojialing granitoids in the formation periods and produced the conjugate shear fracture along the section. Before these fault zones were denuded and exposed on the surface, they were undulating discontinuities in the middle crust with a fluctuation range of 10−18 km; the discontinuities controlled the distribution of gold mineralization and Mesozoic granitic rocks [60,61]. The tectonic evolution of the fault zones is presented in Fig. 11 (the position of this cross section is illustrated by line *IJ* in Fig. 1). The NE-trending ore- controlling fault structures were extended in a nearly parallel way, showing a group of WNW–ESE-trending extensional fault structures horizontally and a combination of gently inclined faults and secondary tensile fractures vertically. Hence, the fault structures in and around the mine area generally feature the concurrent development of primary and secondary faults. During the mineralization, these faults were all normal faults. Due to the relative movement of the upper and lower walls of the main faults, a series of tensile and shear fractures formed in the footwall, and their tendencies were basically opposite to the tendencies of primary fault structures. The footwalls of the Sanshandao–Cangshang fault zone and Jiaojia fault zone show a similar structural feature. The metallogenic process is closely correlated with the NW-directed subduction of the Pacific plate. During the collision between the Pacific plate and Eurasia in the Yanshanian, the gold-rich ancient strata and rocks at the front of the subduction zone were remelted and mixed with the mantle-derived magma to form an upwelling gold-rich mixed magma. Then, the hydrothermal fluid migrated to and concentrated in the rock mass margin; poured into the nearby structural system; infiltrated, diffused, and condensed into the surrounding rocks; finally mineralized at the intersection of fault structures or the transitional point of fault zones along their strikes and/or inclinations [62]. In particular, the secondary extensional structural fault zones that developed in the footwalls of primary fault structures are in favorable locations for the development of stockwork and vein-type gold deposits (Fig. 11 [61]).

As previously mentioned, the Sanshandao–Cangshang and Sanshandao–Sanyuan fault systems are two primary framework structures of the mine area. Combined with the features of these fault structures, the action mode and direction of the crustal stress can be qualitatively determined. The determined average σ_H direction is oblique to the trend of the F2 and Sanshandao–Cangshang fault zones, with a large angle and nearly parallel to the trend of the Sanshandao–Sanyuan fault. The movement of the fault directly shows the tectonic stress state in the region. Recent field surveys have revealed that the Sanshandao–Cangshang fault zone exhibits dextral faulting behavior. Moreover, the quartz grains in the yellow iron sericite in the footwall of the Sanshandao–Sanyuan fault have been sinistrally sheared and dislocated. Under the

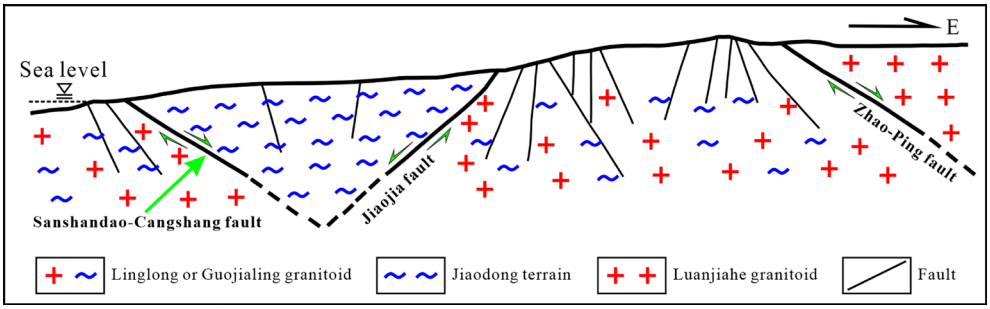

Fig. 11 Tectonic evolution of faults in and around mine area (after DING et al [61])

determined stress states, the NE-trending F2 and Sanshandao–Cangshang faults with dextral characteristics easily form, and the movement of the NW-striking Sanshandao–Sanyuan fault is generally characterized by sinistral strike-slip (Fig. 12), which is in accordance with the conclusions inferred from the geological field survey. The above structural analyses indicate that the mine area is affected by the WNW–ESE or nearly E−W orientation within a contemporary crustal stress setting.

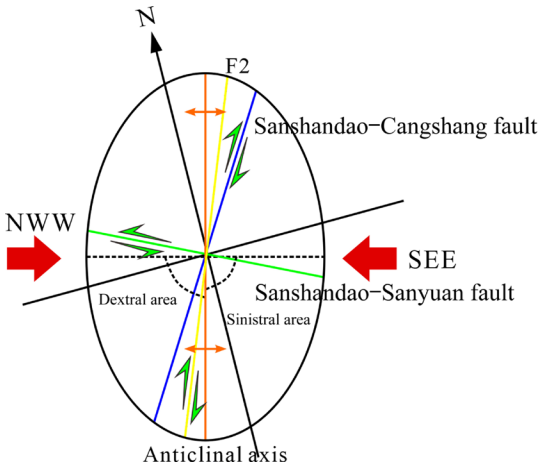

Fig. 12 Sketch map of stress action mode and fault activity characteristics in mine area

Additionally, numerous studies have confirmed that the occurrence of faulting or seismicity is associated with long-term cumulative changes or sudden large changes in the regional crustal stress setting. The possibility of earthquakes induced in areas that are experiencing strong block tectonic movements and appropriate stress conditions is greatly increased. As shown in Figs. 1 and 3, the Jiaodong Peninsula where the gold mine is located, has complicated and multistage fault structures in different directions and is a high-activity area for moderate and small earthquakes in North China. We interpret the occurrence of earthquakes across this area as a consequence of the combined effects of the regional WNW–EW-directed stress field and local NE-directed stress field. For the developed NE-striking faults in the Jiaodong Peninsula, the NE-directed stress field increases the vertical compression on the NE faults, causing stress accumulation, while the WNW–EW-directed stress field decomposes the dextral shear force on the faults, and when the stress release condition is reached, the subsequent fault movement will produce an earthquake. In addition, for the NW-striking faults, the current WNW–EW- or nearly E−W-directed stress conditions can also form high shear stress on the faults, thus causing the faults to undergo sinistral activity. In brief, NE- and NW-striking faults in the Jiaodong Peninsula are the main seismic structures. An example is the Ms 4.6 Laizhou main earthquake in 2013, in which the main activity of the earthquake sequence occurred on the NE-trending Zhacun–Yidao fault, with three small aftershocks occurring on the adjacent NNE-directed fault [63]. The sequence seismogenic faults of the Rushan earthquakes in 2013−2014 are considered to be NW-directed buried strike-slip faults [64]. Moreover, the NW-trending faults in the Bohai Sea (such as the Bohai Sea segment of the Zhangjiakou–Bohai Sea fault zone) have experienced many moderate-strong earthquakes, such as the Ms 3.6 Bohai Sea earthquake in 1980 and Ms 7.4 Bohai Sea earthquake in 1969. These cases are identical to our inference that a WNW−SNN- or approximately E−W-oriented tectonic stress field can trigger fault sliding and generate earthquakes.

In summary, the main function of the early tectonic stress field is the transformation of

geological bodies, resulting in various faults and structures in the rock mass. The early tectonic stress field indirectly controlled the stability of faults, and its residual tectonic stress generally decreased after long-term relaxation, while the contemporary tectonic stress state is the direct mechanical basis that affects the stability of faults. Based on the analysis of the correlations between the tectonic stress field and geological structures in the mine area, the mechanical origin and evolution of the stress field are revealed. Moreover, the stress measurements in this study can be used to explain the action mechanism of fault structures and the formation mechanism of earthquakes around the mine area in practice, and they have good consistency. The consistency between the σ_H direction derived from the measured stress data and neotectonic structures is quite significant, which means that the horizontal stress direction yielded from the recent geological features may be a valuable input to the geomechanical model in the absence of stress measurement data or other data.

It should be noted that due to the complexity of structures in geological bodies, the distribution of tectonic stress can present a very complicated situation, resulting in the possible inconsistency or even obvious differences between the tectonic stress field in local positions or areas and the overall tectonic stress field in a wide area. Furthermore, the present tectonic movement may be considerably different from the early tectonic movement. Therefore, the direction of tectonic stress cannot be determined only from the main regional structures (such as faults), but the current tectonic movement and the local geological structures must be considered, which underscores the necessity of field stress measurements. In addition, shallow stress measurements provide an important basis for analyzing the contemporary crustal stress field and the evolutionary pattern of tectonic movement in and around the mine area. The results also provide new ideas for the study of tectonic evolution activities and the source of driving forces at the land–sea boundary and in the submarine area. The comparison between current stress measurements and geological structural characteristics highlights an important issue, that is, the usefulness of geological structures to indicate the contemporary stress state. However, to understand the links between the crustal stress field and geological structures as well as neotectonic movement more accurately, much field stress measurement work at deeper depths needs to be carried out in the future.

7 Conclusions

(1) The horizontal tectonic stress plays a predominant role in the stress field in the mine area and is a typical tectonic stress field. The stress field is characterized by $\sigma_H>\sigma_h>\sigma_v$ and $\sigma_H>\sigma_v>\sigma_h$, corresponding to the thrust and strike-slip faulting regimes, respectively. With respect to stress magnitudes, the in situ stress level in the mine area is fairly high. The σ_h/σ_v, σ_H/σ_v, and $(\sigma_H+\sigma_h)/(2\sigma_v)$ decrease nonlinearly with increasing depth, and their relationships with depth can be fitted in the form of hyperbolas. The σ_h/σ_v values vary from 0.79 to 1.61, averaging 1.03, the σ_H/σ_v values are between 2.45 and 1.30, averaging 1.58, and the $(\sigma_H+\sigma_h)/(2\sigma_v)$ values mostly range from 1.09 to 1.50, averaging 1.31. As the depth increases, the three coefficients seem to approach the constants of 0.96, 1.45, and 1.20. The σ_H/σ_h values are between 1.16 and 2.11, averaging 1.55, and the values have no significant correlation with depth. The influence of horizontal principal stresses on underground excavations has obvious directionality.

(2) The average σ_H directions measured by overcoring, anelastic strain recovery, and hydraulic fracturing methods are N69.1°W, N59.3°W, and N58.1°W, respectively, which agree well with each other. Overall, the great majority of the measurement points yield a consistent WNW−ESE or approximately E−W orientation for σ_H. This result is quite in line with the orientation of the tectonic stress field derived from focal mechanism solutions, regional geological structural analysis, and other stress indicators revealed by the World Stress Map. This finding suggests that the stress field is significantly influenced by the prevailing WNW-trending tectonic compressive stress, which represents regional stress conditions in and around the mine area.

(3) The tectonic stress field is related to the tectonic movement in the rock stratum and the existing geological structure, especially the horizontal tectonic movement, which has the greatest influence on the formation and distribution characteristics of in situ stress. The current stress field of the mine area basically inherited the

third-stage tectonic stress field (Himalayan movement period) while partially retaining the tectonic stress field characteristics of the second stage (Yanshanian period) and eventually developing into a tectonic stress field featuring nearly E−W compression.

(4) Under the current stress state, the NE-trending F2 and Sanshandao–Cangshang faults with dextral characteristics easily form, and the movement of the NW-striking Sanshandao–Sanyuan fault is generally characterized by sinistral strike-slip, which is in accordance with the conclusions inferred from the geological field survey. Based on the analysis of the correlations between the tectonic stress field and geological structures in the mine area, the mechanical origin and evolution of the regional tectonic stress field are revealed. Moreover, the stress measurements can be employed to explain the action mechanism of fault structures and seismogenesis around the mine area in practice, and they have good consistency, which strongly validates the accuracy of stress measurements.

Acknowledgments

The authors are grateful for the financial supports from the China Postdoctoral Science Foundation (No. 2021M700388), the Interdisciplinary Research Project for Young Teachers of USTB (Fundamental Research Funds for the Central Universities), China (No. FRF-IDRY-20-013), the Fundamental Research Funds for the Central Universities, China (No. FRF-TP-20-041A1), and the National Natural Science Foundation of China (No. U2034206).

References

[1] RAJABI M, TINGAY M, HEIDBACH O. The present-day stress field of New South Wales, Australia [J]. Australian Journal of Earth Sciences, 2016, 63: 1−21.

[2] LI Peng, CAI Mei-feng, GUO Qi-feng, MIAO Sheng-jun. In situ stress state of the northwest region of the Jiaodong Peninsula, China from overcoring stress measurements in three gold mines [J]. Rock Mechanics and Rock Engineering, 2019, 52: 4497−4507.

[3] LI Peng, REN Fen-hua, CAI Mei-feng, GUO Qi-feng, MIAO Sheng-jun. Present-day stress state and fault stability analysis in the capital area of China constrained by in situ stress measurements and focal mechanism solutions [J]. Journal of Asian Earth Sciences, 2019, 185: 104007.

[4] LI Peng, CAI Mei-feng, GUO Qi-feng, REN Fen-hua, MIAO Sheng-jun. Current stress field and its relationship to tectonism in a coal mining district, central China, for underground coal energy exploration [J]. Energy Reports, 2022, 8: 5313−5328.

[5] HEIDBACH O, RAJABI M, CUI Xiao-feng, FUCHS K, MÜLLER B, REINECKER J, REITER K, TINGAY M, WENZEL F, XIE Fu-ren, ZIEGLER M O, ZOBACK M L, ZOBACK M. The world stress map database release 2016: Crustal stress pattern across scales [J]. Tectonophysics, 2018, 744: 484−498.

[6] LI Peng, CAI Mei-feng. Insights into seismicity from the perspective of the crustal stress field: A comment [J]. Natural Hazards, 2022, 111: 1153−1178.

[7] LI Peng, CAI Mei-feng. Assessing the role of absolute stress measurement and relative stress real-time monitoring for earthquake research [J]. Arabian Journal of Geosciences, 2022, 15: 831.

[8] LI Peng, CAI Mei-feng. Challenges and new insights for exploitation of deep underground metal mineral resources [J]. Transactions of Nonferrous Metals Society of China, 2021, 31: 3478−3505.

[9] LI Peng, WU Yun-quan, CAI Mei-feng. Failure behavior of the surrounding rock of jointed rock masses in a gold mine under blasting impact disturbance [J]. Environmental Earth Sciences, 2022, 81: 106.

[10] WU Hao, ZHAO Guo-yan, MA Shao-wei. Failure behavior of horseshoe-shaped tunnel in hard rock under high stress: Phenomenon and mechanisms [J]. Transactions of Nonferrous Metals Society of China, 2022, 32: 639−656.

[11] LI Peng, CAI Mei-feng, GUO Qi-feng, MIAO Sheng-jun. Characteristics and implications of stress state in a gold mine in Ludong area, China [J]. International Journal of Minerals, Metallurgy, and Materials, 2018, 25: 1363−1372.

[12] ZOBACK M L. First- and second-order patterns of stress in the lithosphere: The world stress map project [J]. Journal of Geophysical Research: Solid Earth, 1992, 97: 11703−1128.

[13] ZANG A, STEPHANSSON O, HEIDBACH O, JANOUSCHKOWETZ S. World stress map database as a resource for rock mechanics and rock engineering [J]. Geotechnical and Geological Engineering, 2012, 30: 625−646.

[14] MIAO Sheng-jun, LI Yuan, TAN Wen-hui, REN Fen-hua. Relation between the in-situ stress field and geological tectonics of a gold mine area in Jiaodong Peninsula, China [J]. International Journal of Rock Mechanics and Mining Sciences, 2012, 51: 76−80.

[15] RAJABI M, TINGAY M, HEIDBACH O. The present-day state of tectonic stress in the Darling Basin, Australia: Implications for exploration and production[J]. Marine and Petroleum Geology, 2016, 77: 776−790.

[16] HAN Jun, ZHANG Hong-wei, LIANG Bin, RONG Hai, LAN Tian-wei, LIU Yuan-zheng, REN Ting. Influence of large syncline on in situ stress field: A case study of the Kaiping coalfield, China [J]. Rock Mechanics and Rock Engineering, 2016, 49: 4423−4440.

[17] MIAO Sheng-jun, CAI Mei-feng, GUO Qi-feng, HUANG Zheng-jun. Rock burst prediction based on in-situ stress and

energy accumulation theory [J]. International Journal of Rock Mechanics and Mining Sciences, 2016, 83: 86−94.

[18] LI Peng, CAI Mei-feng, MIAO Sheng-jun, GUO Qi-feng. New insights into the current stress field around the Yishu fault zone, eastern China [J]. Rock Mechanics and Rock Engineering, 2019, 52: 4133−4145.

[19] LIU Xuan, FAN Hong-rui, EVANS N, YANG Kui-feng, DANIŠÍK M, MCINNES B, QIN Ke-zhang, YU Xue-feng. Exhumation history of the Sanshandao Au deposit, Jiaodong: Constraints from structural analysis and (U−Th)/He thermochronology OPEN [J]. Scientific Reports, 2017, 7: 7787.

[20] YAO Bao-kui, LIU Zhu-hua, WANG Jie, ZHANG Cheng-juan, ZENG Xian-qi, FU Hong-ling, LIU Qing-shan. Research on characteristics of field stress in Sanshandao gold mine area [J]. Journal of Engineering Geology, 1995, 3(2): 21−28. (in Chinese)

[21] DENG Jun, YANG Li-qiang, LI Rui-hong, GROVES D I, SANTOSH M, WANG Zhong-liang, SAI Sheng-xun, WANG Si-rui. Regional structural control on the distribution of world-class gold deposits: An overview from the Giant Jiaodong Gold Province, China [J]. Geological Journal, 2019, 54: 378−391.

[22] QIU Zhi-wei, LI Zhan-ke, YUAN Zhong-zheng. Microstructure and trace elements of pyrite from the Sanshandao gold deposit in Jiaodong district: Implications for mechanism of gold enrichment [J]. Earth Science, 2022, 47(1): 290−308. (in Chinese)

[23] HU F F, FAN H R, JIANG X H, LI X C, YANG K F, MERNAGH T. Fluid inclusions at different depths in the Sanshandao gold deposit, Jiaodong Peninsula, China [J]. Geofluids, 2013, 13: 528−541.

[24] MIAO Sheng-jun, WAN Lin-hai, LAI Xing-ping, WANG Shuang-hong. Relation analysis between in-situ stress field and geological tectonism in Sanshandao gold mine [J]. Chinese Journal of Rock Mechanics and Engineering, 2004, 23: 3996−3999. (in Chinese)

[25] LIU Long-long. Characteristic of ore-controlling structure and distribution of mineralization intensity in the Sanshandao gold deposit, Jiaodong Peninsula, China [D]. Beijing: China University of Geosciences (Beijing), 2017. (in Chinese)

[26] LIN Zu-wei, ZHAO Xin-fu, XIONG Le, ZHU Zhao-xian. In-situ trace element analysis characteristics of pyrite in Sanshandao gold deposit in Jiaodong Peninsula: Implications for ore genesis [J]. Advances in Earth Science, 2019, 34: 399−413. (in Chinese)

[27] PAN Su-zhen, WANG Fu-yuan, ZHENG Yan-peng, DUAN Yu-ling, LIU Lan, DENG Xiao-guo, SONG Xiang-hui, SUN Yi-nan, MA Ce-jun, LI Yi-qing. Crustal velocity structure beneath Jiaodong Peninsula and its tectonic implications [J]. Chinese Journal of Geophysics, 2015, 58(9): 3251−3263. (in Chinese)

[28] WANG Hua-lin, GAI Dian-guang, WANG Ji-qiang, GE Fu-gang, ZHONG Pu-yu. Seismic risk assessment of active faults in Zibo city and its adjacent area [J]. Technology for Earthquake Disaster Prevention, 2011, 6(3): 242−256. (in Chinese)

[29] WANG Hua-lin, HU Chao, WANG Ji-qiang, CHEN Ping, LIU Xia. The seismic risk assessment on active faults in Yantai city and its adjacent area [J]. Technology for Earthquake Disaster Prevention, 2015, 10(2): 211−226. (in Chinese)

[30] ZHANG Bin, BAI Xiang-dong, LIU Chen. Preliminary analysis of Ms 4.6 earthquake sequence in Laizhou in Shandong on November 23rd, 2013 [J]. Journal of Institute of Disaster Prevention, 2014, 16(3): 46−52. (in Chinese)

[31] KANG Hong-pu, LIN Jian, YAN Li-xin, ZHANG Xiao, WU Yong-zheng, SI Lin-po. Study on characteristics of underground in-situ stress distribution in Shanxi coal mining fields [J]. Chinese Journal of Geophysicsysics, 2009, 52(7): 1782−1792. (in Chinese)

[32] DONG Xu-guang, ZHOU Cui-ying, HUA Ai-jun. The analysis on focal mechanism solutions of recent minor earthquakes in Bohai straits and its vicinity [J]. Inland Earthquake, 1999, 13(1): 7−16. (in Chinese)

[33] DONG Xu-guang, ZHOU Cui-ying. Circumstance of recent tectonic stress of Yanshan−Bobai Seismic Zone [J]. South China Journal of Seismology, 2000, 20(1): 16−23. (in Chinese)

[34] CAI Mei-feng, HE Man-chao, LIU Dong-yan. Rock mechanics and engineering [M]. Beijing: Science Press, 2002. (in Chinese)

[35] CAI Mei-feng, LIU Wei-dong, LI Yuan. In-situ stress measurement at deep position of Linglong gold mine and distribution law of in-situ stress field in mine area [J]. Chinese Journal of Rock Mechanics and Engineering, 2010, 29(2): 227−233. (in Chinese)

[36] LI Peng, GUO Qi-feng, CAI Mei-feng. Contemporary stress field in and around a gold mine area adjacent to the Bohai Sea, China, and its seismological implications [J]. Bulletin of Engineering Geology and the Environment, 2022, 81: 86.

[37] SJÖBERG J, CHRISTIANSSON R, HUDSON J A. ISRM suggested methods for rock stress estimation — Part 2: overcoring methods [J]. International Journal of Rock Mechanics and Mining Sciences, 2003, 40: 999−1010.

[38] HEIDBACH O, TINGAY M, BARTH A, REINECKER J, KURFEß D, MÜLLER B. Global crustal stress pattern based on the World Stress Map database release 2008 [J]. Tectonophysics, 2010, 482: 3−15.

[39] ZHANG Zhan. Analysis of geostress measurement in Xiling mining area of Sanshandao gold mine [D]. Beijing: Chinese Academy of Geological Sciences, 2021. (in Chinese)

[40] LIN W, KWAŚNIEWSKI M, IMAMURA T, MATSUKI K. Determination of three-dimensional in situ stresses from anelastic strain recovery measurement of cores at great depth [J]. Tectonophysics, 2006, 426: 221−238.

[41] CUI Jun-wei, LIN Wei-ren, WANG Lian-jie, GAO Lu, HUANG Yao, WANG Wei, SUN Dong-sheng, LI Zong-fan, ZHOU Chun-jing, QIAN Hua-shan, PENG Hua, XIA Ke-mei, LI Ke. Determination of three-dimensional in situ stresses by anelastic strain recovery in Wenchuan Earthquake

Fault Scientific Drilling Project Hole-1 (WFSD-1) [J]. Tectonophysics, 2014, 619/620: 123−132.

[42] LIN W R, YEH E C, ITO H, HIRONO T, SOH W, WANG C Y, MA K F, HUNG J H, SONG S R. Preliminary results of stress measurement using drill cores of TCDP hole—A: An application of anelastic strain recovery method to three-dimensional in-situ stress determination [J]. Terrestrial, Atmospheric and Oceanic Sciences, 2007, 18: 379−393.

[43] MATSUKI K, TAKEUCHI K. Three-dimensional in situ stress determination by anelastic strain recovery of a rock core [J]. International Journal of Rock Mechanics and Mining Sciences & Geomechanics Abstracts, 1993, 30: 1019−1022.

[44] SUN Dong-sheng, LYU Hai-tao, WANG Lian-jie, CUI Jun-wen, HE Bi-zhu, CAO Zi-cheng, QIU Hua-biao, YAN Xiu-gang. Determination of the in-situ stress state at 7 km depth under Tarim Basin by ASR and DITH methods [J]. Chinese Journal of Rock Mechanics and Engineering, 2018, 37(2): 383−391. (in Chinese)

[45] RAJABI M, TINGAY M, HEIDBACH O, HILLIS R, REYNOLDS S. The present-day stress field of Australia [J]. Earth-Science Reviews, 2017, 168: 165−189.

[46] HAIMSON B C, LEE M Y, SONG I. Shallow hydraulic fracturing measurements in Korea support tectonic and seismic indicators of regional stress [J]. International Journal of Rock Mechanics and Mining Sciences, 2003, 40: 1243−1256.

[47] ZHAO X G, WANG J, CAI M, MA L K, ZONG Z H, WANG X Y, SU R, CHEN W M, ZHAO H G, CHEN Q C, AN Q M, QIN X H, OU M Y, ZHAO J S. In-situ stress measurements and regional stress field assessment of the Beishan area, China [J]. Engineering Geology, 2013, 163: 26−40.

[48] ZHAO X G, WANG J, QIN X H, CAI M, SU R, HE J G, ZONG Z H, MA L K, JI R L, ZHANG M, ZHANG S, YUN L, CHEN Q C, NIU L L, AN Q M. In-situ stress measurements and regional stress field assessment in the Xinjiang candidate area for China's HLW disposal [J]. Engineering Geology, 2015, 197: 42−56.

[49] KANG H, ZHANG X, SI L, WU Y, GAO F. In-situ stress measurements and stress distribution characteristics in underground coal mines in China [J]. Engineering Geology, 2010, 116: 333−345.

[50] LI Peng, MIAO Sheng-jun. Analysis and application of in-situ stress in metal mining area of Chinese mainland [J]. Chinese Journal of Engineering, 2017, 39(3): 323−334. (in Chinese)

[51] LI Peng, CAI Mei-feng. Distribution law of in situ stress field and regional stress field assessments in the Jiaodong Peninsula, China [J]. Journal of Asian Earth Sciences, 2018, 166: 66−79.

[52] YU Xue-fu, ZHENG Ying-ren, LIU Huai-heng, FANG Zheng-chang. Stability analysis of surrounding rock mass in underground engineering [M]. Beijing: Coal Industry Publishing House, 1983. (in Chinese)

[53] XIE He-ping, GAO Feng, JU Yang. Research and development of rock mechanics in deep ground engineering [J]. Chinese Journal of Rock Mechanics and Engineering, 2015, 34(11): 2161−2178. (in Chinese)

[54] LIU Quan-sheng, LIU Kai-de. Characteristics of in-situ stress field for deep levels in Huainan coal mine [J]. Rock and Soil Mechanics, 2012, 33(7): 2089−2096. (in Chinese)

[55] BROWN E T, HOEK E. Trends in relationships between measured in-situ stresses and depth [J]. International Journal of Rock Mechanics and Mining Sciences & Geomechanics Abstracts, 1978, 15: 211−215.

[56] WANG Cheng-hu, ZHANG Yan-shan, GUO Qi-liang, ZHAO Shi-guang. New integrated analysis method to analyze stress regime of engineering area [J]. Chinese Journal of Geotechnical Engineering, 2011, 33(10): 1562−1568. (in Chinese)

[57] XIE Fu-ren, ZHANG Hong-yan, CUI Xiao-feng, DU Yi. The modern tectonic stress field and strong earthquakes in China [J]. Recent Developments in World Seismology, 2011, 41: 4−12. (in Chinese)

[58] LI Yong, ZHONG Jian-hua, WEN Zhi-feng, DUAN Hong-liang, WANG Hai-qiao. Effects of Indosinian movements on tectonic formation and evolution, Jiyang depression [J]. Geological Review, 2006, 52(3): 321−330. (in Chinese)

[59] WAN Tian-feng, TEYSSIER C, ZENG Hua-lin, ZHOU Wei-xin, TIKOFF B. Emplacement mechanism of Linglong granitoid complex, Shandong Peninsula, China [J]. Science in China Series D: Earth Sciences, 2001, 44: 535−544.

[60] SUN Feng-yue. Mesozoic−Cenozoic regional tectonic evolution and gold mineralization in Jiaodong area, Shandong Province [J]. Journal of Changchun University of Earth Sciences, 1994, 24(4): 378−384. (in Chinese)

[61] DING Zheng-jiang, SUN Feng-yue, LIU Fu-lai, LIU Jian-hui, PENG Qi-ming, JI Pan, LI Bi-le, ZHANG Pi-jian. Mesozoic geodynamic evolution and metallogenic series of major metal deposits in Jiaodong Peninsula, China [J]. Acta Petrologica Sinica, 2015, 31(10): 3045−3080. (in Chinese)

[62] ZHAO Dong-dong, JIN Gang, LI Hai-song, HUANG Ji-you. Geological characteristics of Sanshandao island gold deposit in Laizhou, Shandong Province and the genetic discussion [J]. Contributions to Geology and Mineral Resources Research, 2013, 28(4): 546−551. (in Chinese)

[63] ZHENG Jian-chang, LI Dong-mei, WANG Peng, ZHAO Jin-hua, XU Chang-peng. A preliminary discussion on the focal mechanism and seismic tectonic feature of the 2013 Laizhou M4.6 earthquake sequence [J]. Seismology and Geology, 2015, 37(2): 384−399. (in Chinese)

[64] QU Jun-hao, JIANG Hai-kun, LI Jin, ZHANG Zhi-hui, ZHENG Jian-chang, ZHANG Qin. Preliminary study for seismogenic structure of the Rushan earthquake sequence in 2013—2014 [J]. Chinese Journal of Geophysics, 2015, 58(6): 1954−1962. (in Chinese)

华北地区莱州湾沿海金矿区现今构造应力状态及构造作用

李 鹏[1,2,3]，郭奇峰[1,2,3]，蔡美峰[1,2,3]，苗胜军[1,2,3]

1. 北京科技大学 土木与资源工程学院，北京 100083；
2. 北京科技大学 金属矿山高效开采与安全教育部重点实验室，北京 100083；
3. 北京科技大学 城市地下空间工程北京市重点实验室，北京 100083

摘 要：为了研究华北地区莱州湾附近沿海金矿区的现今构造应力状态和构造作用，采用应力解除法、滞弹性应变恢复法和水压致裂法开展地应力测量工作，共测定 49 组地应力数据。结果表明，水平构造应力在现今应力场中占主导地位，是一种典型的构造应力场。应力场的特征为 $\sigma_H>\sigma_h>\sigma_v$ (σ_H、σ_h 和 σ_v 分别为最大水平主应力、最小水平主应力和垂直主应力)和 $\sigma_H>\sigma_v>\sigma_h$，这分别有利于逆冲和走滑断裂活动。应力水平相对较高，不利于地下结构的稳定性。σ_H 的方向为 WNW–ESE 或近 E−W 向，这与震源机制解和区域地质构造分析的结果一致。现今应力场是不同地质时期动力作用和构造运动的结果，研究区的应力场总体上继承了第三期 (喜马拉雅运动期) 构造应力场的特征，同时部分保留了第二期(燕山期)构造应力场的特征，最终演化为以近 E−W 向挤压为特征的构造应力场。

关键词：地应力测量；现今应力场；构造作用；断裂构造；沿海金矿区

(Edited by Wei-ping CHEN)